International Journal of Solids and Structures 52 (2015) 1–18

Contents lists available at ScienceDirect

International Journal of Solids and Structures

journal homepage: www.elsevier.com/locate/ijsolstr

A finite element implementation of a coupled diffusion-deformation theory for elastomeric gels

Shawn A. Chester [a,*], Claudio V. Di Leo [b], Lallit Anand [b]

[a] Department of Mechanical and Industrial Engineering, New Jersey Institute of Technology, Newark, NJ 07102, USA
[b] Department of Mechanical Engineering, Massachusetts Institute of Technology, Cambridge, MA 02139, USA

ARTICLE INFO

Article history:
Received 11 March 2014
Received in revised form 15 July 2014
Available online 28 August 2014

Keywords:
Elastomeric materials
Gels
Diffusion
Large deformations
Finite elements

ABSTRACT

The theory of Chester and Anand (2011) for fluid diffusion and large deformations of elastomeric gels is implemented as a user-defined element (UEL) subroutine in the commercial finite element software package ABAQUS. A specialized form of the constitutive equations and the governing partial differential equations of the theory are summarized, and the numerical implementation is described in detail. To demonstrate the robustness of the numerical implementation a few illustrative numerical simulation examples for axisymmetric, plane strain, and three-dimensional geometries are shown. For educational purposes, and also to facilitate the numerical implementation of other coupled multiphysics theories, the source code for the UEL is provided as an online supplement to this paper.

1. Introduction

An elastomeric gel is a polymer network swollen by a fluid. Gels can be designed to swell by several hundred percent in volume, and the amount of swelling can be controlled by varying various stimuli—humidity, temperature, and pH. Gels are ubiquitous—they are found in foods and medicines, and they find use in several important and diverse applications including carriers for drug delivery (Peppas et al., 2006), actuators and sensors in microfluidic devices (Beebe et al., 2000), tissue engineering matrices (Chan and Mooney, 2008), as well as packers for sealing in oil wells (Kleverlaan et al., 2005; Bhavsar et al., 2008).

Modeling elastomeric gels is interesting and challenging—it involves concurrent deformation of the polymer network and diffusion of the solvent through the network. An early, but limited, theory for swelling of gels is due to Tanaka and co-workers (cf., e.g., Tanaka and Fillmore, 1979). In recent years there has been a convergence towards a more complete coupled diffusion-deformation theory for describing the response of gels—including swelling and drying, squeezing of fluid by applied mechanical deformation, and forced permeation (cf., e.g., Doi, 2009). Within the limits of a nonlinear field theory in which the fluid–solid mixture is treated as a single homogenized continuum body which allows for a mass flux of the fluid, essentially similar theories (for electrically-neutral gels) have been formulated by Hong et al. (2008), Duda et al. (2010) and Chester and Anand (2010, 2011). References to the vast previous literature on gels may be found in these publications.

The past few years have also seen several publications related to the numerical implementation of these theories for solving coupled diffusion-deformation boundary value problems for gels. In their early work, Suo and co-workers (cf., e.g., Hong et al., 2009; Marcombe et al., 2010; Liu et al., 2010) using the UHYPER capabilities of the commercial finite element package ABAQUS/Standard (2013) implemented a "*chemical equilibrium*" version their theory in which the chemical potential was presumed to be homogeneous in the gel, and the transient diffusion and associated transient swelling kinetics were neglected. More recently, Toh et al. (2013) and Duan et al. (2013) have simulated the transient diffusion and swelling kinetics of polymeric gels by drawing on an analogy between diffusion of solvent molecules and conduction of heat in solids, and using the built-in thermo-mechanically coupled finite-elements and associated solution procedures in ABAQUS. While useful for gels in which the diffusion equation has a form similar to that for heat transfer, this methodology is not applicable to more general multi-physics problems. In addition to UHYPER capabilities, Zhang et al. (2009) developed a finite element method for gels based on the theory presented in Hong et al. (2008). Lucantonio et al. (2013)—using the finite element software package COMSOL/Multiphysics—have also recently performed simulations for transient swelling-induced large deformations in polymeric gels.

In contrast to the work of Suo et al., Toh et al. (2013), and Lucantonio et al. (2013), Chester and Anand (2011) implemented their own theory for elastomeric gels by writing two- and

* Corresponding author. Tel.: +1 973 596 3658.
E-mail address: shawn.a.chester@njit.edu (S.A. Chester).

http://dx.doi.org/10.1016/j.ijsolstr.2014.08.015
0020-7683/

three-dimensional user-defined finite element subroutines (UELs) and implemented them in ABAQUS. In their approach, a new finite element is constructed whose degrees of freedom are taken to be the primal variables in the set of partial differential equations (pdes) of interest. This set of pdes *need not resemble* those for coupled thermo-mechanical problems, and may be of any kind which are amenable to finite-element solutions methods which employ standard $\mathcal{C}^0$-continuous finite-element basis functions.

Because detailed numerical procedures and source codes are seldom published in scientific journal papers, the numerical implementation of a new coupled theory using the finite element method is often a challenging task—especially for beginners in a new research area. However there is a new emerging trend—in order to more widely disseminate new computational methods and procedures—researchers are beginning to publish papers which address the details of their computational implementations. For example, recently Giner et al. (2009) published an ABAQUS implementation of the extended finite element method for linear elastic fracture analysis as a UEL subroutine. Also Park and Paulino (2012) published an ABAQUS implementation of a cohesive finite element as a UEL subroutine. In both cases, for *educational purposes*, the numerical implementation is discussed in detail, and the source code for the UEL was provided.

In Chester and Anand (2011) we showed the results from several numerical simulations of our theory which was implemented as a user-defined element (UEL) subroutine in ABAQUS. However, in that paper we did not provide any details regarding our numerical implementation procedures and methods. Accordingly, in the spirit of the recent papers by Giner et al. (2009) and Park and Paulino (2012), the main purpose of this paper is to discuss the details of the numerical implementation of our coupled diffusion-deformation theory for non-ionic gels, and also to make available the source code for the UEL in ABAQUS.

The paper is organized as follows. In Section 2 the constitutive equations and the governing partial differential equations of the theory are summarized. In order to focus attention on the numerical implementation as opposed to the details of the specific constitutive functions, we use a simple specialized form of our constitutive theory and restrict our discussion to isothermal conditions. In Section 3 we describe the numerical solution procedure in substantial detail. Additional details regarding the user elements, verification of the basic element technology, and thermo-chemo-mechanical coupling is provided in three Appendices.

- The associated online Supplemental materials to this paper include a detailed tutorial on generating an input file, and instructions on running ABAQUS with our UEL. The source code is also provided.

In Section 4, in order to demonstrate the robustness of the numerical implementation, we show the results from illustrative example problems for axisymmetric, plane strain, and three-dimensional geometries. We finish in Section 5 with some concluding remarks.

2. Summary of our theory for gels

In this section we briefly summarize the basic continuum mechanical theory for elastomeric gels under isothermal conditions. Cf. Chester and Anand (2011) for complete details of the formulation of the theory.

2.1. Kinematics. Constitutive theory

Consider a fluid-free (dry) macroscopically homogeneous elastomeric body. We identify such a macroscopically-homogeneous body B with the region of space it occupies in a fixed reference configuration, and denote by $\mathbf{X}$ an arbitrary material point of B. A motion of B is then a smooth one-to-one mapping $\mathbf{x}=\boldsymbol{\chi}(\mathbf{X},t)$ with deformation gradient, velocity, and velocity gradient given by[1]

$$\mathbf{F}=\nabla\boldsymbol{\chi},\quad \mathbf{v}=\dot{\boldsymbol{\chi}},\quad \mathbf{L}=\operatorname{grad}\mathbf{v}=\dot{\mathbf{F}}\mathbf{F}^{-1}. \tag{2.1}$$

The deformed body is denoted as $\mathcal{B}$.

The theory is based upon a multiplicative decomposition

$$\mathbf{F}=\mathbf{F}^e\mathbf{F}^s,\quad \text{with}\quad \mathbf{F}^s=\lambda^s\mathbf{1},\quad \lambda^s>0, \tag{2.2}$$

of the deformation gradient $\mathbf{F}$ into elastic and swelling parts $\mathbf{F}^e$ and $\mathbf{F}^s$, respectively, with the swelling taken to be isotropic, where λ^s is the swelling stretch. With Ω denoting the volume of a mole of fluid molecules, we assume the swelling stretch is given by

$$\lambda^s=(1+\Omega c_{\mathrm{R}})^{1/3}, \tag{2.3}$$

where c_{R} represents the *fluid concentration* measured in moles of fluid per unit reference volume of the dry elastomer.

The constitutive equations of the theory are:

- *Free energy*: A simple form of the free energy function which accounts for the combined effects of mixing, swelling, and elastic stretching is,

$$\psi_{\mathrm{R}}=\mu^0 c_{\mathrm{R}}+R\vartheta c_{\mathrm{R}}\left(\ln\left(\frac{\Omega c_{\mathrm{R}}}{1+\Omega c_{\mathrm{R}}}\right)+\chi\left(\frac{1}{1+\Omega c_{\mathrm{R}}}\right)\right)+\frac{1}{2}G(3(\bar{\lambda}^2-1)-2\ln J)+J^s\left[\frac{1}{2}K(\ln J^e)^2\right]. \tag{2.4}$$

  Here, μ^0 is a reference chemical potential for the fluid, R the gas constant, ϑ is the *constant* temperature under consideration, χ is a dimensionless measure of the "enthalpy" of mixing known as the Flory–Huggins interaction parameter, G is the shear modulus of the network, K is a bulk modulus of the gel, and

$$\bar{\lambda}\overset{\text{def}}{=}\sqrt{\frac{1}{3}\operatorname{tr}\mathbf{C}}=\sqrt{\frac{1}{3}(1+\Omega c_{\mathrm{R}})^{2/3}\operatorname{tr}\mathbf{C}^e}, \tag{2.5}$$

  is an *effective stretch*.
- *Constitutive equation for the Cauchy stress*: Corresponding to the free energy (2.4), the Cauchy stress $\mathbf{T}$ is given by

$$\mathbf{T}=J^{-1}\left(2\mathbf{F}^e\frac{\partial\psi_{\mathrm{R}}}{\partial\mathbf{C}^e}\mathbf{F}^{e\top}\right)=J^{-1}\left[G\phi^{-2/3}\mathbf{B}^e-G\mathbf{1}+J^sK(\ln J^e)\mathbf{1}\right], \tag{2.6}$$

  where we have introduced the *polymer volume fraction* defined by

$$\phi\overset{\text{def}}{=}\frac{1}{1+\Omega c_{\mathrm{R}}}=(\lambda^s)^{-3}. \tag{2.7}$$

  Next, since

$$\mathbf{B}(\equiv\mathbf{F}\mathbf{F}^{\top})=(\lambda^s)^2\mathbf{B}^e=\phi^{-2/3}\mathbf{B}^e, \tag{2.8}$$

  (2.6) reduces to

$$\mathbf{T}=J^{-1}\left[G(\mathbf{B}-\mathbf{1})+J^sK(\ln J^e)\mathbf{1}\right]. \tag{2.9}$$

[1] Notation: We use standard notation of modern continuum mechanics (Gurtin et al., 2010). Specifically: ∇ and Div denote the gradient and divergence with respect to the material point $\mathbf{X}$ in the reference configuration; grad and div denote these operators with respect to the point $\mathbf{x}=\boldsymbol{\chi}(\mathbf{X},t)$ in the deformed body; a superposed dot denotes the material time-derivative. Throughout, we write $\mathbf{F}^{e-1}=(\mathbf{F}^e)^{-1}$, $\mathbf{F}^{e-\top}=(\mathbf{F}^e)^{-\top}$, etc. We write $\operatorname{tr}\mathbf{A}$, $\operatorname{sym}\mathbf{A}$, $\operatorname{skw}\mathbf{A}$, $\mathbf{A}_0$, and $\operatorname{sym}_0\mathbf{A}$ respectively, for the trace, symmetric, skew, deviatoric, and symmetric-deviatoric parts of a tensor $\mathbf{A}$. Also, the inner product of tensors $\mathbf{A}$ and $\mathbf{B}$ is denoted by $\mathbf{A}:\mathbf{B}$, and the magnitude of $\mathbf{A}$ by $|\mathbf{A}|=\sqrt{\mathbf{A}:\mathbf{A}}$.

- *Constitutive equation for the chemical potential*: The chemical potential μ is given by

$$\mu = \frac{\partial \psi_{\mathrm{R}}}{\partial c_{\mathrm{R}}} - \Omega \frac{1}{3} J^e \mathrm{tr}\mathbf{T} = \mu^0 + R\vartheta\left(\ln(1-\phi) + \phi + \chi\phi^2\right) - \Omega K(\ln J^e) + \frac{1}{2} K\Omega(\ln J^e)^2. \tag{2.10}$$

- *Constitutive equation for the fluid flux*: We assume that the spatial fluid flux, $\mathbf{j}$, depends linearly on the spatial gradient of the chemical potential, $\mathrm{grad}\,\mu$, with the mobility tensor taken to be isotropic so that

$$\mathbf{j} = -m\,\mathrm{grad}\,\mu, \tag{2.11}$$

where m is a scalar mobility coefficient, which in general is an isotropic function of the stretch and the fluid concentration.

Remark. In our previous papers (Chester and Anand, 2010; Chester and Anand, 2011; Chester, 2012) we had assumed a constitutive equation for the fluid flux of the form

$$\mathbf{j}_{\mathrm{R}} = -m\nabla\mu,$$

where $\mathbf{j}_{\mathrm{R}}$ is a referential fluid flux and $\nabla\mu$ is the referential gradient of the chemical potential. However, others in the literature (c.f., e.g., Hong et al., 2008; Duda et al., 2010) have argued that (2.11) is the more appropriate constitutive equation for the fluid flux for isotropic gels. We adopt (2.11) in this paper.

2.2. Governing partial differential equations

The governing partial differential equations, when expressed in the deformed body, consist of

1. The local force balance for the macroscopic Cauchy stress,

$$\mathrm{div}\mathbf{T} + \mathbf{b} = \mathbf{0}, \tag{2.12}$$

with $\mathbf{b}$ a non-inertial body force, and $\mathbf{T}$ given by (2.9).

2. The local balance for the fluid concentration,

$$\dot{c}_{\mathrm{R}} = -J\mathrm{div}\mathbf{j}, \tag{2.13}$$

which using (2.7) may be written in the form

$$\frac{\dot{\phi}}{J\Omega\phi^2} - \mathrm{div}\mathbf{j} = 0, \tag{2.14}$$

in which the fluid flux $\mathbf{j}$ is given by (2.11), and the chemical potential μ is given by (2.10).

2.3. Boundary and initial conditions

We also need boundary and initial conditions to complete the theory. Let $\mathcal{S}_{\mathbf{u}}$ and $\mathcal{S}_{\mathbf{t}}$ be complementary subsurfaces of the boundary $\partial\mathcal{B}$ of the body $\mathcal{B}$ in the sense $\partial\mathcal{B} = \mathcal{S}_{\mathbf{u}} \cup \mathcal{S}_{\mathbf{t}}$ and $\mathcal{S}_{\mathbf{u}} \cap \mathcal{S}_{\mathbf{t}} = \varnothing$. Similarly let $\mathcal{S}_{\mu}$ and $\mathcal{S}_{\mathbf{j}}$ be complementary subsurfaces of the boundary: $\partial\mathcal{B} = \mathcal{S}_{\mu} \cup \mathcal{S}_{\mathbf{j}}$ and $\mathcal{S}_{\mu} \cap \mathcal{S}_{\mathbf{j}} = \varnothing$. Then for a time interval $t \in [0,T]$ we consider a pair of boundary conditions in which the displacement $\mathbf{u}$ is specified on $\mathcal{S}_{\mathbf{u}}$ and the surface traction on $\mathcal{S}_{\mathbf{t}}$:

$$\left.\begin{aligned} \mathbf{u} &= \breve{\mathbf{u}} \quad \text{on } \mathcal{S}_{\mathbf{u}} \times [0,T], \\ \mathbf{T}\mathbf{n} &= \breve{\mathbf{t}} \quad \text{on } \mathcal{S}_{\mathbf{t}} \times [0,T]; \end{aligned}\right\} \tag{2.15}$$

and a pair of boundary conditions in which the chemical potential is specified on $\mathcal{S}_{\mu}$ and the fluid flux on $\mathcal{S}_{\mathbf{j}}$

$$\left.\begin{aligned} \mu &= \breve{\mu} \quad \text{on } \mathcal{S}_{\mu} \times [0,T], \\ -\mathbf{j}\cdot\mathbf{n} &= \breve{j} \quad \text{on } \mathcal{S}_{\mathbf{j}} \times [0,T]; \end{aligned}\right\} \tag{2.16}$$

with $\breve{\mathbf{u}}, \breve{\mathbf{t}}, \breve{\mu}, \breve{j}$, *prescribed* functions of $\mathbf{x}$ and t. The initial data is taken as

$$\mathbf{u}(\mathbf{X},0) = \mathbf{u}_0(\mathbf{X}), \quad \text{and} \quad \mu(\mathbf{X},0) = \mu_0(\mathbf{X}) \quad \text{in B}. \tag{2.17}$$

The coupled set of Eqs. (2.12) and (2.14), together with (2.15), (2.16), and (2.17) yield an initial boundary value problem for the displacement $\mathbf{u}(\mathbf{x},t)$ and the chemical potential $\mu(\mathbf{x},t)$.

In applications, for the case in which the environment consists of a pure and incompressible liquid, the boundary condition on chemical potential $\breve{\mu}$ is given by

$$\breve{\mu} = \mu^0 + \Omega p_a, \tag{2.18}$$

where μ^0 is a reference chemical potential for the liquid, Ω is the volume of a mole of liquid molecules, and p_a is the hydrostatic pressure of the liquid. Also, if a portion of the boundary is impermeable to the liquid, then on that portion the prescribed normal flux $\breve{j}$ vanishes.

3. Numerical solution procedure

In the absence of body forces, the strong forms of the coupled partial differential equations of the theory are

$$\text{Balance of momentum} \begin{cases} \mathrm{div}\mathbf{T} = \mathbf{0} & \text{in } \mathcal{B}, \\ \mathbf{u} = \breve{\mathbf{u}} & \text{on } \mathcal{S}_{\mathbf{u}}, \\ \mathbf{T}\mathbf{n} = \breve{\mathbf{t}} & \text{on } \mathcal{S}_{\mathbf{t}}, \end{cases}$$

$$\text{Balance of fluid concentration} \begin{cases} \dfrac{\dot{\phi}}{J\Omega\phi^2} - \mathrm{div}\mathbf{j} = 0 & \text{in } \mathcal{B}, \\ \mu = \breve{\mu} & \text{on } \mathcal{S}_{\mu}, \\ -\mathbf{j}\cdot\mathbf{n} = \breve{j} & \text{on } \mathcal{S}_{\mathbf{j}}. \end{cases} \tag{3.1}$$

Then, with $\mathbf{w}_1, w_2$ denoting two weighting (or test) fields which vanish on $\mathcal{S}_{\mathbf{u}}$ and $\mathcal{S}_{\mu}$, respectively, the corresponding weak forms are:

$$\left.\begin{aligned} \int_{\mathcal{B}} \left(\mathbf{T} : \frac{\partial \mathbf{w}_1}{\partial \mathbf{x}}\right) dv &= \int_{\mathcal{S}_{\mathbf{t}}} (\mathbf{w}_1 \cdot \breve{\mathbf{t}}) da, \\ \int_{\mathcal{B}} \left(w_2 \frac{\dot{\phi}}{J\Omega\phi^2}\right) dv &= -\int_{\mathcal{B}} \left(\frac{\partial w_2}{\partial \mathbf{x}} \cdot \mathbf{j}\right) dv - \int_{\mathcal{S}_{\mathbf{j}}} \left(w_2 \breve{j}\right) da. \end{aligned}\right\} \tag{3.2}$$

The body is approximated using finite elements, $\mathcal{B} = \bigcup \mathcal{B}^e$, and the trial solutions for the displacement, and chemical potential are interpolated inside each element by

$$\left.\begin{aligned} \mathbf{u} &= \sum \mathbf{u}^A N^A, \\ \mu &= \sum \mu^A N^A, \end{aligned}\right\} \tag{3.3}$$

with the index $A = \{1, 2, \ldots, M\}$ denoting the nodes of the element, $\mathbf{u}^A$, and μ^A denoting nodal displacements, and chemical potentials, and N^A the shape functions. We employ a standard Galerkin approach, in that the weighting fields are interpolated by the same shape functions, viz.

$$\left.\begin{aligned} \mathbf{w}_1 &= \sum \mathbf{w}_1^A N^A, \\ w_2 &= \sum w_2^A N^A. \end{aligned}\right\} \tag{3.4}$$

Using (3.3) and (3.4) in (3.2) yields the following element-level system of equations:

$$\left.\begin{aligned} \int_{\mathcal{B}^e} \left(\mathbf{T} \frac{\partial N^A}{\partial \mathbf{x}}\right) dv &= \int_{\mathcal{S}_{\mathbf{t}}^e} \left(N^A \breve{\mathbf{t}}\right) da, \\ \int_{\mathcal{B}^e} \left(N^A \frac{\dot{\phi}}{J\Omega\phi^2}\right) dv &= -\int_{\mathcal{B}^e} \left(\frac{\partial N^A}{\partial \mathbf{x}} \cdot \mathbf{j}\right) dv - \int_{\mathcal{S}_{\mathbf{j}}^e} \left(N^A \breve{j}\right) da. \end{aligned}\right\} \tag{3.5}$$

This system of coupled equations is solved using a Newton procedure by defining the following element-level residuals for the displacement and chemical potential,

$$\left.\begin{aligned}(\mathbf{R_u})^A &= -\int_{\mathcal{B}^e}\left(\mathbf{T}\frac{\partial N^A}{\partial \mathbf{x}}\right)dv + \int_{\mathcal{S}^e_{\mathbf{t}}}\left(N^A\check{\mathbf{t}}\right)da,\\ (R_\mu)^A &= \int_{\mathcal{B}^e}\left(N^A\frac{\dot\phi}{J\Omega\phi^2}\right)dv + \int_{\mathcal{B}^e}\left(\frac{\partial N^A}{\partial \mathbf{x}}\cdot\mathbf{j}\right)dv + \int_{\mathcal{S}^e_{\mathbf{j}}}\left(N^A\check{j}\right)da,\end{aligned}\right\} \tag{3.6}$$

which using index notation, and (2.11) for the fluid flux, may be written in the form

$$\left.\begin{aligned}(R_{u_i})^A &= -\int_{\mathcal{B}^e}\left(T_{ij}\frac{\partial N^A}{\partial x_j}\right)dv + \int_{\mathcal{S}^e_{\mathbf{t}}}\left(N^A\check{t}_i\right)da,\\ (R_\mu)^A &= \int_{\mathcal{B}^e}\left(N^A\frac{\dot\phi}{J\Omega\phi^2}\right)dv - \int_{\mathcal{B}^e}\left(m\frac{\partial N^A}{\partial x_i}\frac{\partial \mu}{\partial x_i}\right)dv + \int_{\mathcal{S}^e_{\mathbf{j}}}\left(N^A\check{j}\right)da.\end{aligned}\right\} \tag{3.7}$$

In addition to the residuals, the following tangents are also required for the iterative Newton solver:

$$\left.\begin{aligned}(\mathbf{K_{uu}})^{AB} &= -\frac{\partial(\mathbf{R_u})^A}{\partial \mathbf{u}^B},\\ (\mathbf{K}_{\mathbf{u}\mu})^{AB} &= -\frac{\partial(\mathbf{R_u})^A}{\partial \mu^B},\\ (\mathbf{K}_{\mu\mathbf{u}})^{AB} &= -\frac{\partial(R_\mu)^A}{\partial \mathbf{u}^B},\\ (K_{\mu\mu})^{AB} &= -\frac{\partial(R_\mu)^A}{\partial \mu^B}.\end{aligned}\right\} \tag{3.8}$$

First, the tangent $(3.8)_1$, in index notation, is given by

$$K^{AB}_{u_iu_k} = \int_{\mathcal{B}^e}\frac{\partial N^A}{\partial x_j}(\mathbb{A}_{ijkl})\frac{\partial N^B}{\partial x_l}dv - \int_{\mathcal{S}^e_{\mathbf{t}}}N^AN^B\frac{\partial \check{t}_i}{\partial u_k}da. \tag{3.9}$$

With $\mathbf{T}_{\mathrm{R}} = J\mathbf{T}\mathbf{F}^{-\top}$ denoting the Piola stress, the *spatial tangent modulus* $\mathbb{A}$ is defined in terms of the *referential tangent modulus* $\mathbb{A}_{\mathrm{R}}$ by

$$\mathbb{A}_{ijkl} \overset{\text{def}}{=} J^{-1}F_{jm}F_{ln}(\mathbb{A}_{\mathrm{R}})_{imkn}, \tag{3.10}$$

where

$$\mathbb{A}_{\mathrm{R}} = \frac{\partial \mathbf{T}_{\mathrm{R}}}{\partial \mathbf{F}}. \tag{3.11}$$

This standard result requires lengthy computations, which we give in an appendix (cf. the Remark in Appendix A). For the constitutive theory under consideration here, using the constitutive equation (2.9) for $\mathbf{T}$ we obtain that

$$\mathbf{T}_{\mathrm{R}} = G(\mathbf{F}-\mathbf{F}^{-\top}) + J^sK(\ln J^e)\mathbf{F}^{-\top}, \tag{3.12}$$

and hence

$$\mathbb{A}_{\mathrm{R}} = \frac{\partial \mathbf{T}_{\mathrm{R}}}{\partial \mathbf{F}} = G\left(\mathbb{I} - \frac{\partial \mathbf{F}^{-\top}}{\partial \mathbf{F}}\right) + J^sK\left(\mathbf{F}^{-\top}\otimes\frac{\partial \ln J}{\partial \mathbf{F}} + (\ln J^e)\frac{\partial \mathbf{F}^{-\top}}{\partial \mathbf{F}}\right), \tag{3.13}$$

where in writing the last term in (3.13) we have used $\ln J^e = \ln(J\phi) = \ln J + \ln\phi$. Then using the identities

$$(\mathbb{I})_{ijkl} = \delta_{ik}\delta_{jl}, \quad \left(\frac{\partial \mathbf{F}^{-\top}}{\partial \mathbf{F}}\right)_{ijkl} = -F^{-1}_{li}F^{-1}_{jk}, \quad \left(\frac{\partial \ln J}{\partial \mathbf{F}}\right)_{kl} = F^{-1}_{lk}, \tag{3.14}$$

the component form of the referential tangent modulus is

$$(\mathbb{A}_{\mathrm{R}})_{ijkl} = \left(\frac{\partial \mathbf{T}_{\mathrm{R}}}{\partial \mathbf{F}}\right)_{ijkl} = G\left(\delta_{ik}\delta_{jl} + F^{-1}_{li}F^{-1}_{jk}\right) + J^sK\left(F^{-1}_{ji}F^{-1}_{lk} - (\ln J^e)F^{-1}_{li}F^{-1}_{jk}\right). \tag{3.15}$$

Consider next the tangent $(3.8)_4$,

$$\begin{aligned}K^{AB}_{\mu\mu} &= -\int_{\mathcal{B}^e}\frac{N^A}{J\Omega}\frac{\partial}{\partial \mu^B}\left(\frac{\dot\phi}{\phi^2}\right)dv + \int_{\mathcal{B}^e}\frac{\partial}{\partial \mu^B}\left(m\frac{\partial N^A}{\partial x_i}\frac{\partial \mu}{\partial x_i}\right)dv\\ &\quad - \int_{\mathcal{S}^e_{\mathbf{j}}}\frac{\partial}{\partial \mu^B}\left(N^A\check{j}\right)da,\\ &= -\int_{\mathcal{B}^e}\frac{N^A}{J\Omega}\left(-2\frac{\dot\phi}{\phi^3}\frac{\partial \phi}{\partial \mu^B} + \frac{1}{\phi^2}\frac{\partial \dot\phi}{\partial \mu^B}\right)dv + \int_{\mathcal{B}^e}\left(m\frac{\partial N^A}{\partial x_i}\frac{\partial N^B}{\partial x_i}\right)dv\\ &\quad + \int_{\mathcal{B}^e}\left(\frac{\partial m}{\partial \mu^B}\frac{\partial N^A}{\partial x_i}\frac{\partial \mu}{\partial x_i}\right)dv - \int_{\mathcal{S}^e_{\mathbf{j}}}\left(N^A\frac{\partial \check{j}}{\partial \mu^B}\right)da,\end{aligned}$$

and hence

$$\begin{aligned}K^{AB}_{\mu\mu} &= \int_{\mathcal{B}^e}\frac{N^AN^B}{J\Omega\phi^2}\left(2\frac{\dot\phi}{\phi}\frac{\partial \phi}{\partial \mu} - \frac{\partial \dot\phi}{\partial \mu}\right)dv + \int_{\mathcal{B}^e}\left(m\frac{\partial N^A}{\partial x_i}\frac{\partial N^B}{\partial x_i}\right)dv\\ &\quad + \int_{\mathcal{B}^e}\left(\frac{\partial m}{\partial \mu}N^B\frac{\partial N^A}{\partial x_i}\frac{\partial \mu}{\partial x_i}\right)dv - \int_{\mathcal{S}^e_{\mathbf{j}}}\left(N^AN^B\frac{\partial \check{j}}{\partial \mu}\right)da.\end{aligned} \tag{3.16}$$

Similarly, the remaining two tangents in (3.8) are given by

$$K^{AB}_{u_i\mu} = \int_{\mathcal{B}^e}\frac{\partial N^A}{\partial x_j}\left(\frac{\partial T_{ij}}{\partial \phi}\frac{\partial \phi}{\partial \mu}\right)N^Bdv, \tag{3.17}$$

where

$$\frac{\partial \mathbf{T}}{\partial \phi} = \frac{K}{J^e\phi}\mathbf{1},$$

and $(\mathbf{K}_{\mu\mathbf{u}})^{AB}$ is approximated by

$$K^{AB}_{\mu u_k} = -\int_{\mathcal{B}^e}\frac{\partial N^A}{\partial x_i}\left(m\frac{\partial \mu}{\partial x_k}\delta_{il}\right)\frac{\partial N^B}{\partial x_l}dv. \tag{3.18}$$

In the solution procedure one needs to compute the polymer volume fraction, ϕ, at every increment in order to evaluate the constitutive response functions and eventually the residuals (3.6). Using $J^e = J\phi$ we may rewrite (2.10) in the following dimensionless form

$$\frac{\mu^0-\mu}{R\vartheta} + \ln(1-\phi) + \phi + \chi\phi^2 - \frac{\Omega K}{R\vartheta}\ln(J\phi) + \frac{1}{2}\frac{\Omega K}{R\vartheta}\ln(J\phi)^2 = 0, \tag{3.19}$$

which serves as an implicit equation for ϕ. Thus given the pair $(\mathbf{F}, \mu)$ at any instant of time, Eq. (3.19) is solved for the corresponding value of ϕ. The term $\dot\phi$ is computed using the approximation,

$$\dot\phi = \frac{\phi_{n+1}-\phi_n}{\Delta t}. \tag{3.20}$$

Also, terms such as $\partial\dot\phi/\partial\mu$ appearing in the tangents (3.16) are computed numerically using a finite difference scheme.

In (3.6), (3.9) and (3.16) the integrals are evaluated numerically using Gaussian-quadrature. Since this is a standard method in the finite element literature, we do not present details here; the details may be found in our source code and in the literature.

In its' notation, ABAQUS/Standard (2013) requires certain matrices denoted as `RHS` and `AMATRX` to be evaluated and/or updated by the user element subroutine UEL:

- The matrix `RHS`, as defined by the ABAQUS documentation, is "An array containing the contributions of this element to the right-hand-side vectors of the overall system of equations." Referring to (3.7), `RHS` is the overall elemental residual which in *matrix form* is given by

$$\mathsf{R} = \left[R^1_{u_1}\ R^1_{u_2}\ R^1_{\mu}\ R^2_{u_1}\ R^2_{u_2}\ R^2_{\mu}\ldots R^M_{u_1}\ R^M_{u_2}\ R^M_{\mu}\right]^{\top}, \tag{3.21}$$

in two dimensions, and

$$\mathrm{R} = \left[R^1_{u_1}\ R^1_{u_2}\ R^1_{u_3}\ R^1_{\mu}\ R^2_{u_1}\ R^2_{u_2}\ R^2_{u_3}\ R^2_{\mu} \ldots R^M_{u_1}\ R^M_{u_2}\ R^M_{u_3}\ R^M_{\mu}\right]^{\top}, \tag{3.22}$$

in three dimensions, with M the total number of nodes per element.

- The matrix AMATRX as defined by the ABAQUS documentation is "An array containing the contribution of this element to the Jacobian (stiffness) or other matrix of the overall system of equations." Referring to (3.8), AMATRX is the overall tangent which is given by

$$\mathrm{K} = \begin{bmatrix} K^{11}_{u_1u_1} & K^{11}_{u_1u_2} & K^{11}_{u_1\mu} & K^{12}_{u_1u_1} & K^{12}_{u_1u_2} & K^{12}_{u_1\mu} & & K^{1M}_{u_1u_1} & K^{1M}_{u_1u_2} & K^{1M}_{u_1\mu} \\ K^{11}_{u_2u_1} & K^{11}_{u_2u_2} & K^{11}_{u_2\mu} & K^{12}_{u_2u_1} & K^{12}_{u_2u_2} & K^{12}_{u_2\mu} & & K^{1M}_{u_2u_1} & K^{1M}_{u_2u_2} & K^{1M}_{u_2\mu} \\ K^{11}_{\mu u_1} & K^{11}_{\mu u_2} & K^{11}_{\mu\mu} & K^{12}_{\mu u_1} & K^{12}_{\mu u_2} & K^{12}_{\mu\mu} & & K^{1M}_{\mu u_1} & K^{1M}_{\mu u_2} & K^{1M}_{\mu\mu} \\ K^{21}_{u_1u_1} & K^{21}_{u_1u_2} & K^{21}_{u_1\mu} & K^{22}_{u_1u_1} & K^{22}_{u_1u_2} & K^{22}_{u_1\mu} & \cdots & K^{2M}_{u_1u_1} & K^{2M}_{u_1u_2} & K^{2M}_{u_1\mu} \\ K^{21}_{u_2u_1} & K^{21}_{u_2u_2} & K^{21}_{u_2\mu} & K^{22}_{u_2u_1} & K^{22}_{u_2u_2} & K^{22}_{u_2\mu} & & K^{2M}_{u_2u_1} & K^{2M}_{u_2u_2} & K^{2M}_{u_2\mu} \\ K^{21}_{\mu u_1} & K^{21}_{\mu u_2} & K^{21}_{\mu\mu} & K^{22}_{\mu u_1} & K^{22}_{\mu u_2} & K^{22}_{\mu\mu} & & K^{22}_{\mu u_1} & K^{2M}_{\mu u_2} & K^{2M}_{\mu\mu} \\ & & & \vdots & & & \ddots & & \vdots & \\ K^{M1}_{u_1u_1} & K^{M1}_{u_1u_2} & K^{M1}_{u_1\mu} & K^{M2}_{u_1u_1} & K^{M2}_{u_1u_2} & K^{M2}_{u_1\mu} & & K^{MM}_{u_1u_1} & K^{MM}_{u_1u_2} & K^{MM}_{u_1\mu} \\ K^{M1}_{u_2u_1} & K^{M1}_{u_2u_2} & K^{M1}_{u_2\mu} & K^{M2}_{u_2u_1} & K^{M2}_{u_2u_2} & K^{M2}_{u_2\mu} & \cdots & K^{MM}_{u_2u_1} & K^{MM}_{u_2u_2} & K^{MM}_{u_2\mu} \\ K^{M1}_{\mu u_1} & K^{M1}_{\mu u_2} & K^{M1}_{\mu\mu} & K^{M2}_{\mu u_1} & K^{M2}_{\mu u_2} & K^{M2}_{\mu\mu} & & K^{MM}_{\mu u_1} & K^{MM}_{\mu u_2} & K^{MM}_{\mu\mu} \end{bmatrix} \tag{3.23}$$

in two dimensions. For brevity we do not list the complete matrix in three dimensions.

In addition to the required RHS and AMATRX as described above, ABAQUS/Standard (2013) allows the storage and updating state variables using SVARS, which as defined by the ABAQUS documentation is "An array containing the values of the solution-dependent variables associated with this element." Due to the term $\dot{\phi}$ appearing in (3.7), and computed using (3.20), we are required to save ϕ at each integration point. For that purpose we use the SVARS(Variables) array (where the length Variables is set in the input file) to save ϕ in the form

$$\mathrm{SVARS} = \left[\phi_1\ \phi_2\ \phi_3 \ldots \phi_{\mathrm{Q}}\right], \tag{3.24}$$

where Q is the total number of integration points in the element.

We have also used the PNEWDT time-step control feature of ABAQUS. PNEWDT as defined by the ABAQUS/Standard (2013) documentation is "Ratio of suggested new time increment to the time increment currently being used." If PNEWDT is set less than 1.0, ABAQUS will abandon the current increment and start over with a new time increment DTIME of DTIME×PNEWDT for the next time increment. If PNEWDT is set greater than 1.0, and the increment converges, ABAQUS may increase the next time increment DTIME by DTIME×PNEWDT. In this work we make extensive use of PNEWDT, it is used for both general time incrementation as well as constitutive time incrementation. An example of constitutive time incrementation is limiting the local change in the polymer volume fraction ϕ in a given time step. Also, if a displacement increment, or chemical potential increment is too large PNEWDT is used to decrease the time increment. Further details may be found in the source code.

We have implemented our theory in ABAQUS/Standard (2013) by writing a user element subroutine (UEL) by writing three different elements:

(i) a 2D plane-strain 4-node linear isoparametric quadrilateral which we refer to as UPE4;
(ii) a 2D axisymmetric 4-node linear isoparametric quadrilateral which we refer to as UAX4; and
(iii) a 3D 8-node linear isoparametric brick which we refer to as U3D8.

Additional details regarding the user elements is provided in Appendix A, and the basic element technology is verified in Appendix B.

- The associated online Supplemental materials to this paper include a detailed tutorial on generating an input file, and instructions on running ABAQUS with our UEL. The source code is also provided.

4. Example problems

To demonstrate the robustness of the developed user element subroutine (UEL), in this section we show a few illustrative numerical simulation examples for plane strain, axisymmetric, and three-dimensional geometries. Table 1 lists plausible representative values for the material properties of a polymeric gel at room temperature, which we have used in our calculations.

Specifically, the ground state shear modulus for the polymer, G, is chosen to have a value 1 MPa, and the bulk modulus K is taken to be two orders of magnitude larger. The volume of a solvent molecule is taken as $\Omega = 1.0 \times 10^{-4}$ m^3/mol, and the reference chemical potential of the fluid is taken as $\mu^0 = 0.0$ J/mol. Additionally, we have chosen a value of $\chi = 0.1$ for the Flory–Huggins interaction parameter—a value which is favorable for a high degree of swelling.

Recall that the mobility m in (2.11) is an isotropic function of the stretch and the fluid content. We assume here that the mobility at a given temperature ϑ is given by[2]

$$m = \frac{Dc}{R\vartheta}, \tag{4.1}$$

where $D > 0$, a constant, represents a diffusion coefficient, and $c = c_{\mathrm{R}}/J$ is the fluid concentration measured in moles of fluid per unit deformed volume. As a representative value in our numerical simulations we take $D = 5 \times 10^{-9}$ m^2/s.

4.1. Free-swelling of an axisymmetric cylinder followed by simple compression between rigid platens

We first consider free-swelling of a cylindrical sample of an initially dry gel, followed by simple compression of the swollen gel between rigid platens.[3] We simulate compression between rigid platens (as opposed to simple tension) in order illustrate the use of our UEL with the contact capabilities of ABAQUS.

The initially-dry cylindrical specimen is 5 mm in diameter and 5 mm tall. In our numerical simulation we assume an axisymmetric initial cylindrical geometry shown in Fig. 1. Using symmetry, we model only half of an axisymmetric slice and approximate it by using 175 UAX4 user-elements; the mesh is purposely chosen to be unstructured. The compression platen (not shown) is modeled as a rigid surface. Finally, to study frictional boundary effects between the swollen gel and the rigid surface we consider two cases: (i) the interface between the gel and the platen is frictional with a Coulomb friction coefficient of $\mu_{\mathrm{fric}} = 0.05$, and (ii) a frictionless case with $\mu_{\mathrm{fric}} = 0.0$.

The simulation is broken into two steps: in Step 1 the initially dry gel is allowed to freely swell to a near equilibrium cylindrical

[2] At present not much is known experimentally about the precise dependence of m on either the stretch or the fluid content, we use this simple form to describe our numerical solution procedure.

[3] Cai et al. (2010) have recently performed such experiments on an alginate hydrogel.

Table 1
Material parameters for a representative elastomeric gel at room temperature.

Parameter	Value
G	1 MPa
K (=100G)	100 MPa
Ω	1.0×10^{-4} m^3/mol
χ	0.1
μ^0	0.0 J/mol
D	5×10^{-9} m^2/s

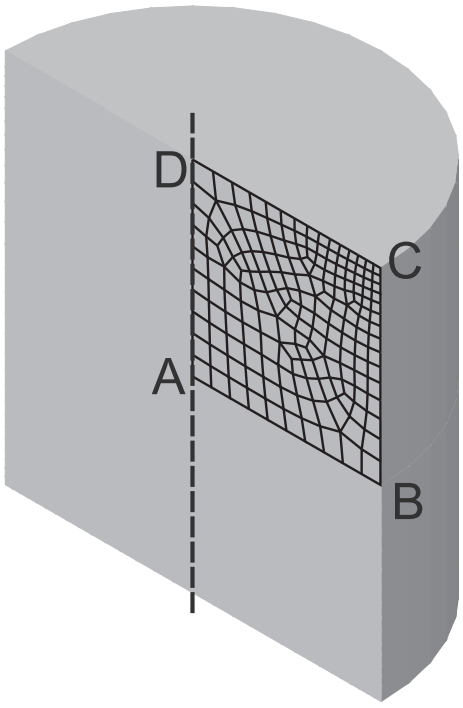

Fig. 1. Initial geometry used in the free swelling followed by simple compression example. Here only half the geometry is shown for clarity, and the finite element mesh superimposed. Due to symmetry, only half of an axisymmetric slice is modeled.

shape, and in Step 2 the rigid platen is moved into the swollen gel to compress it. The initial condition for the chemical potential of the dry polymer is taken to be

$$\mu(\mathbf{X}, t = 0) = \mu_0 = -14388.57 \text{ J/mole}. \tag{4.2}$$

This initial condition is computed using Eq. (2.10), with $\mu^0 = 0.0$ J/mole, $\phi = 0.999, \vartheta = 298$ K, $J^e = 1.0$, and $\chi = 0.1$.[4] The boundary conditions are as follows:

- Step 1:
  - For the mechanical boundary conditions we prescribe $u_r = 0$ along AD, $u_z = 0$ along AB, while faces BC and CD are taken to be traction-free. In this step, the rigid surface is sufficiently removed from the specimen and held fixed.
  - For the chemical boundary conditions we prescribe zero flux along AD and AB due to symmetry, while faces BC and CD are prescribed a time dependent chemical potential

    $$\breve{\mu}(t) = \mu^0 + \mu_0 \exp(-t/t_d),$$

    where μ^0 is the chemical potential of the surrounding solvent and $t_d = 300$ s, so that at times $t \gg t_d$ the prescribed chemical potential $\breve{\mu}(t)$ approaches the value $\mu^0 = 0.0$ J/mole of the surrounding solvent.
  - The total time allowed for this swelling step is 6 h. At which point the swelling gel has come into contact with the rigid platen.
- Step 2:
  - For the mechanical boundary conditions, symmetry conditions $u_r = 0$ along AD and $u_z = 0$ along AB are maintained from the previous step, however now the rigid surface is prescribed an additional downward displacement of 2.5 mm over 300 s, and then held fixed in the displaced position for another 6 h.
  - For the chemical boundary conditions we maintain the zero flux conditions along AD and AB, however now we add a no flux boundary condition to face CD which is in contact with the rigid surface. Face BC maintains the boundary condition $\breve{\mu} = \mu^0$ with the solvent.

In Fig. 2,

- Fig. 2(a) and (b) show snapshots of the polymer volume fraction ϕ plotted on the deformed geometry in the free-swelling step after 3 h and 6 h, respectively, of swelling.
- For the case with a Coulomb friction $\mu_{\text{fric}} = 0.05$, Fig. 2(c) and (d) show snapshots of the polymer volume fraction ϕ plotted on the deformed geometry after 220 s and 6 h, respectively, in the second compression step.
- For the frictionless case $\mu_{\text{fric}} = 0.0$, Fig. 2(e) and (f) show snapshots of the polymer volume fraction ϕ plotted on the deformed geometry after 220 s and 6 h, respectively, in the second compression step.

The redistribution of the fluid due to the compression is clearly observed in Fig. 2—an indication of the coupling between the deformation and diffusion. Also, in the frictional case in the long time limit Fig. 2 (d), the region of low ϕ (more swollen) near the edges of the gel is due to a region of tensile stress relative to the surroundings—the "tensile" stress in this region develops due to the friction between the gel and the platen. In contrast, in the frictionless case, Fig. 2 (f), the distribution of the polymer volume fraction ϕ along the direction of compression is much more uniform—as expected.

The force–displacement and force–time curves computed during Step 2 are shown in Fig. 3 for the frictionless case.[5] Since the underlying material model for the polymer is fully elastic, the apparent "stress relaxation" seen in Fig. 3(b) is due entirely to the out-flux of fluid.

This first illustrative numerical example shows the use of our axisymmetric user-element undergoing large deformations, transient fluid transport, and frictional contact with a rigid surface.

4.2. Constrained swelling of a bilayer in plane strain

This example problem is modeled after the recent experiments of Yoon et al. (2010) which are similar to the experiments of Holmes and co-workers (Holmes et al., 2011; Pandey and Holmes, 2013). In the experiments of Yoon et al. (2010) a thin layer of a swellable gel is bonded to a non-swellable elastomer, the gel is allowed to swell and this causes large bending of the bilayer.

The initial dry geometry is taken to be 100 mm long and 5 mm tall, with 2.5 mm for the swellable gel and 2.5 mm for the

[4] We have used $\phi(\mathbf{X}, t = 0)$=0.999 rather than 1.0 to eliminate numerical difficulties with the $\ln(1 - \phi)$ term in (2.10).

[5] The corresponding curves for the frictional case are not much different.

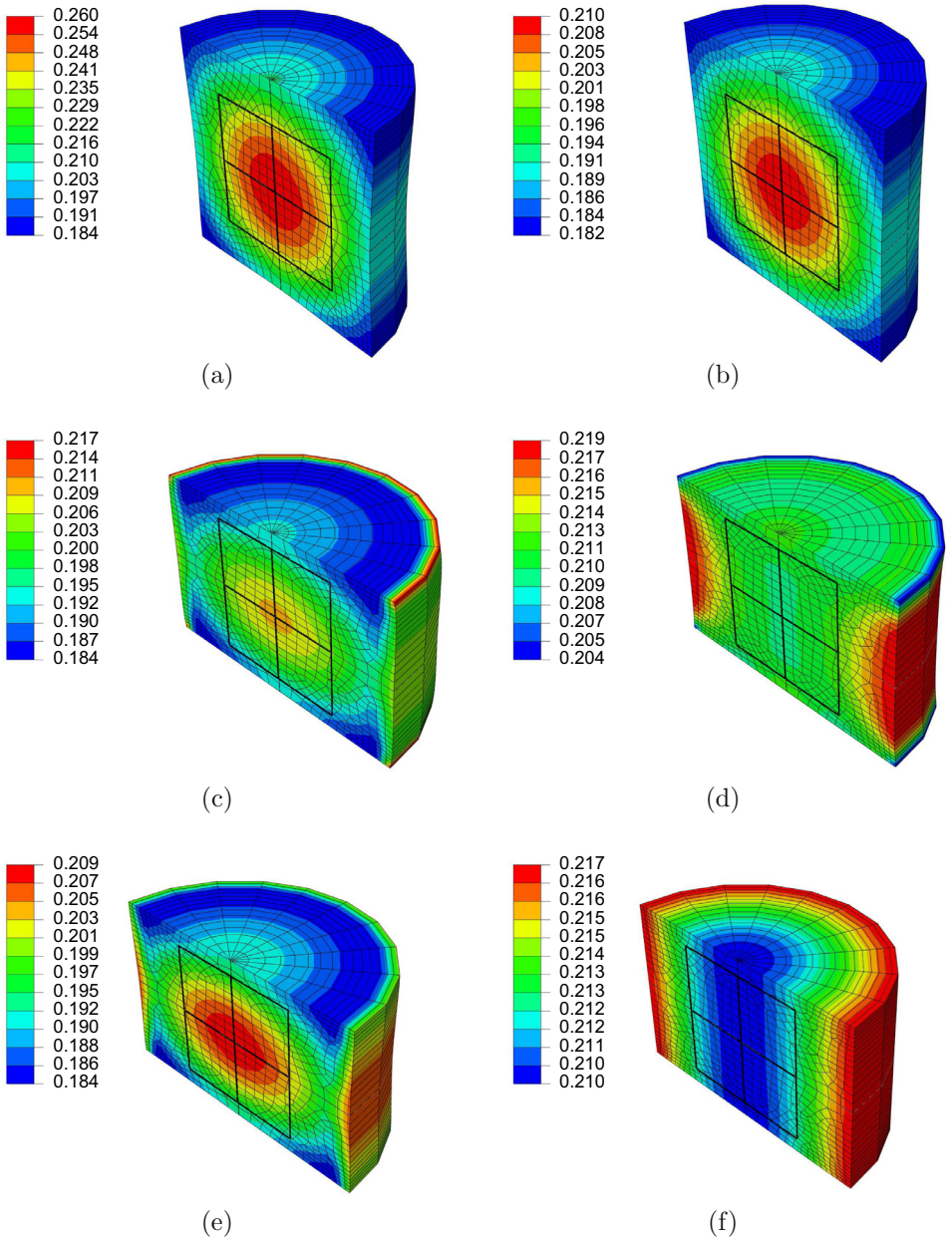

Fig. 2. Contours of the polymer volume fraction ϕ on the deformed body at (a) after 3 h of free swelling, (b) after 6 h of free swelling, (c) after 220 s of compression, and (d) 6 h after the compression platen has been held fixed in the deformed position with a Coulomb friction coefficient of 0.05. For comparison, considering a frictionless interface between the platen and gel, after (e) 220 s of compression, and (f) 6 h after the compression platen has been held fixed in the deformed position. For clarity the rigid surface has been removed, and the axisymmetric mesh swept and mirrored about symmetry lines/planes. The thick black lines indicate the initial dry body.

non-swellable elastomeric substrate. Due to the symmetry of the problem, we only model one-half of the geometry in the simulation, Fig. 4; we assume that plane strain conditions prevail. The swellable gel is approximated by 201 UPE4 plane strain user-elements, while the non-swellable elastomer is approximated by 201 CPE4H 4-node plane strain hybrid elements (built-in ABAQUS elements). The non-swellable elastomer is modeled as an incompressible Neo-Hookean material with a shear modulus of 50 MPa. The interface between the gel and non-swellable elastomer is taken to be perfectly bonded.

As in the previous example, the initial condition for the chemical potential of the dry swellable gel is taken to be $\mu(\mathbf{X}, t = 0) = \mu_0 = -14388.57$ J/mol. Referring to Fig. 4, for the mechanical boundary conditions we impose symmetry along the symmetry plane of the beam (face AD), and pin the node at point A to avoid rigid body motion. The free end of the beam (face BC) is constrained to remain planar, and all other faces are traction free. For the chemical boundary conditions we prescribe no flux along the plane of symmetry AD. The top face of the beam CD is prescribed a uniform time dependent chemical potential of $\breve{\mu}(t) = \mu^0 + \mu_0 \exp(-t/t_d)$, with $t_d = 300$ s.

Fig. 5(a)–(d) shows snapshots of the polymer volume fraction ϕ on the deformed beam after 15 min, 30 min, 1 h, and 6 h, respectively.[6]

This numerical example shows the use of our plane strain user elements in conjunction with built-in ABAQUS plane-strain elements.

[6] Note that since we model only half the geometry in the finite element simulation, the self contact shown in Fig. 5(d) is modeled by the use of a rigid surface which is not shown in this figure.

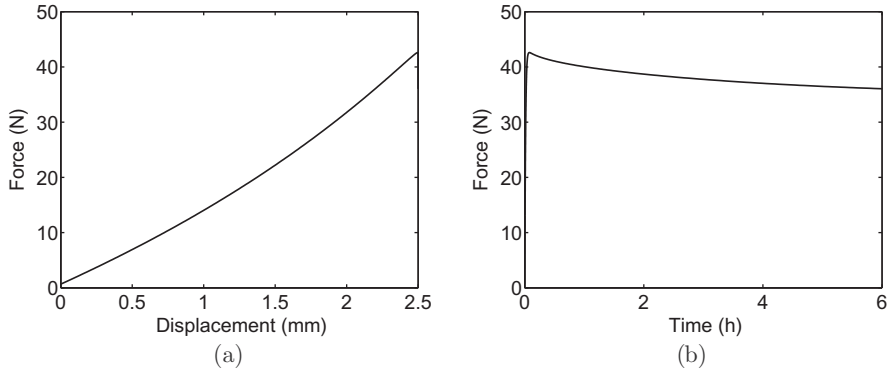

Fig. 3. (a) Force – displacement response, and (b) force – time response for the simple compression simulation. The small offset from the origin in the force displacement curve is due to a small preload during the swelling step. Also, note the force relaxation due to the movement of the fluid within the body.

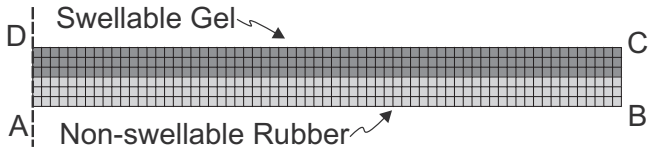

Fig. 4. Initial geometry used in the constrained swelling example. Here only half the geometry is simulated due to symmetry. The swellable gel is the darker material above and the non-swellable rubber is the lighter material below.

4.3. Swelling induced three-dimensional buckling of constrained cylindrical tubes

This final example problem is modeled after the recent experiments conducted by Lee et al. (2012) on hydrogel tubes. Their experiments consisted of cylindrical tubes of hydrogels which were mechanically constrained on one end, while the other end was placed in contact with a fluid and allowed to swell and possibly buckle. In their experiments Lee et al. (2012) varied the geometry of their tubes and found that varying the wall thickness, radii, and heights of their tubes resulted in the formation of different "buckled" patterns on the swollen ends of their hydrogel tubes.

Due to the nature of the experimentally-observed three-dimensional buckled patterns, we model the body in three dimensions. Fig. 6 shows the basic geometry under consideration, a tube with outer diameter D_0, wall thickness t_0, and height H_0 in the initial dry configuration. We consider two initial geometries:

$$\{D_0, t_0, H_0\} = \{4.636, 0.206, 0.6\}\,\text{mm} \quad \text{and} \quad \{4.636, 0.309, 1.2\}\,\text{mm}$$

for our numerical simulations. These dimensions were chosen to provide two distinct swollen shapes similar to those reported in the recent paper of Lee et al. (2012). Guided by the (approximate) symmetry observed in their experiments, we model only 1/4 of the geometry. The initial meshes are shown in Fig. 6, they consist of 2720, and 6840 U3D8 8-node brick elements with 4 and 6 elements through the thickness for the "short" and "tall" geometries, respectively. In order to aid the initiation of buckling, all nodes on the front face of the cylindrical body were given a small random geometric imperfection on the order 10^{-2} mm in the height dimension.

As in the previous examples, the initial condition for the chemical potential of the dry swellable gel is taken to be $\mu(\mathbf{X}, t = 0) = \mu_0 = -14388.57$ J/mole. For the mechanical boundary conditions, referring to Fig. 6, we assume that the back face is held fixed, all symmetry planes are prescribed appropriate symmetry conditions, and the remaining faces are traction free. For the chemical boundary conditions, we assume that only the front face is in contact with the fluid, and prescribe $\breve{\mu}(t) = \mu^0 + \mu_0 \exp(-t/t_d)$ with $t_d = 300$ s while all other faces are flux free.

Fig. 7 shows contours of the polymer volume fraction on the deformed body after 215 s, 250 s, and 900 s, for (a) the "short-thin" tube and (b) the "tall-thick" tube. These shapes resemble those

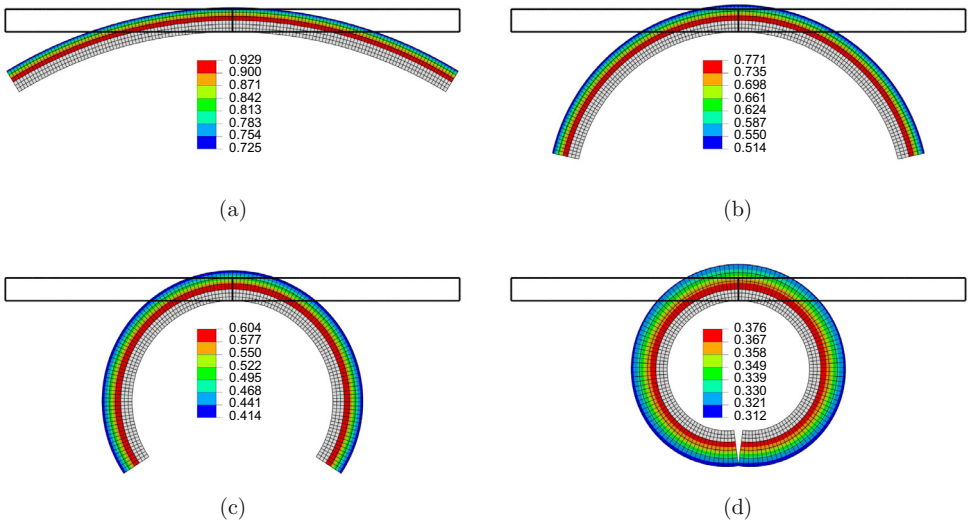

Fig. 5. Contours of the polymer volume fraction ϕ on the deformed body at (a) 15 min, (b) 30 min, (c) 1 h, and (d) 6 h. The initial dry geometry is shown by the thick black lines and the non-swellable rubber is shown on the deformed mesh in white.

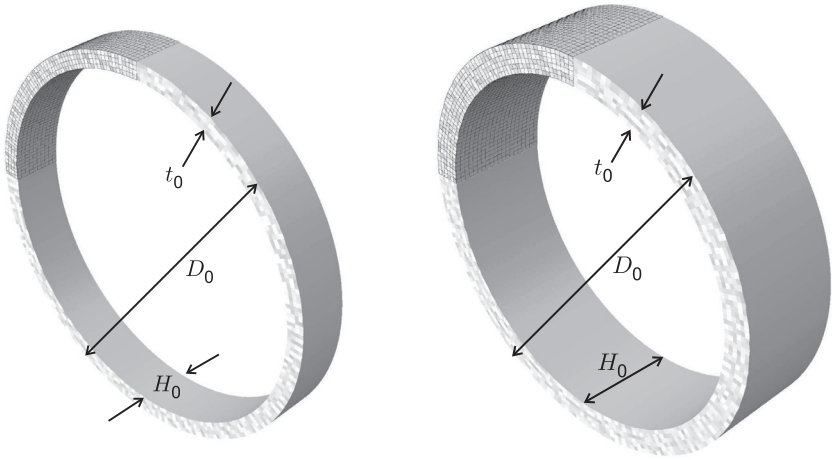

Fig. 6. Initial geometries used in the swell induced buckling simulations. Only one-quarter of the geometry is meshed and symmetry boundary conditions are assumed.

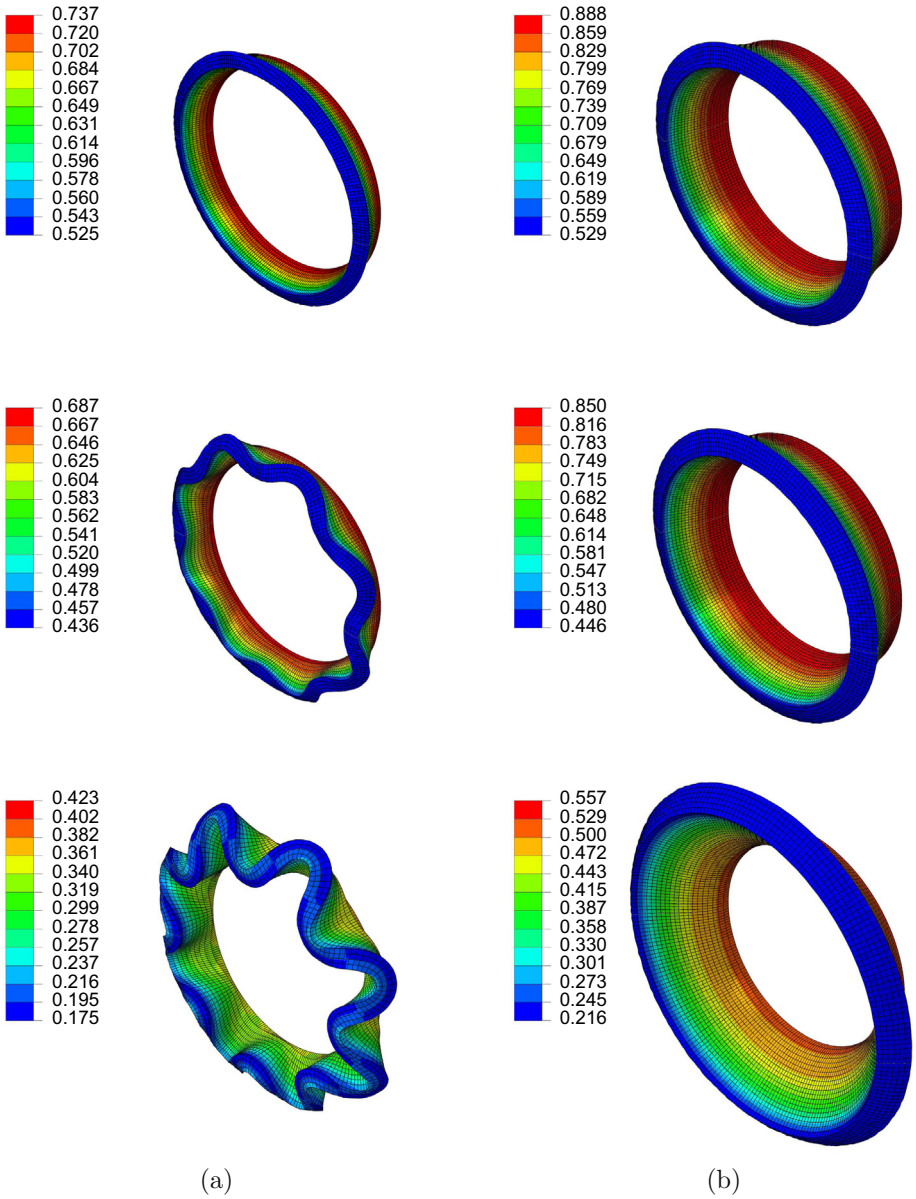

Fig. 7. Contours of the polymer volume fraction ϕ on the deformed body for $\{D_0, t_0, H_0\}$ given by (a) $\{4.636, 0.206, 0.6\}$ mm and (b) $\{4.636, 0.361, 1.825\}$ mm, at 215 s (top), 250 s (middle), and 900 s (bottom) of swelling. Note how the initial geometry leads to very different swollen shapes, one buckled and the other stable.

observed experimental by Lee et al. (2012), and we note that the initial geometry in Fig. 7(a) results in a "buckled" pattern, while the initial geometry in Fig. 7(b) results in an axisymmetrically swollen tube.

These simulation results show that our three-dimensional user-element is able to capture the differing deformed shapes in the two geometries.

5. Concluding remarks

The coupled theory of Chester and Anand (2011) for fluid permeation and large deformations of elastomeric gels is implemented as a user-defined element (UEL) subroutine in ABAQUS/Standard (2013). The numerical solution procedure employing a user element (UEL) in ABAQUS is discussed in significant detail, and the online Supplemental materials to this paper include a detailed tutorial on generating an input file, and instructions on running ABAQUS with our UEL. The source code is also provided.

Further, in an Appendix, Section C, we overview a thermo-chemo-mechanically coupled theory for thermally responsive gels. That Appendix serves as an example on how to extend the material shown in the main body of this paper to another theory and implementation. The source code for the thermo-chemo-mechanically coupled theory is also provided.

It is hoped that the details of the numerical implementation of the particular coupled diffusion-deformation theory for gels provided here, will also facilitate the numerical implementation of other coupled multi-physics theories within the ABAQUS framework via user elements.

Indeed, the finite element framework described here has already proven useful in the numerical implementation of a variety of other theories in ABAQUS: (a) gradient plasticity (Anand et al., 2012); (b) oxide growth in thermal barrier coatings (Loeffel et al., 2013; Al-Athela et al., 2013); (c) dielectric elastomers (Henann et al., 2013); (d) surface tension in soft materials (Henann and Bertoldi, 2014); (e) hydrogen transport in metals (Di Leo and Anand, 2013); and Lithium diffusion in electrode materials (Di Leo et al., 2014).

Acknowledgements

The financial support provided by a grant from the National Science Foundation (CMMI-1063626) is gratefully acknowledged. Also, SAC gratefully acknowledges Suvrat P. Lele as a mentor who provided initial guidance in programming UEL subroutines for ABAQUS, and Kaspar Loeffel for finding many of the initial flaws in his code.

Appendix A. Isoparametric elements

A.1. Basic element technology

Typically, in finite element formulations the volume (meaning non-surface) contribution to the displacement residual $(3.7)_1$ is evaluated in matrix form

$$\mathsf{R}_{\mathbf{u}} = -\int_{\mathcal{B}^e} \mathsf{B}^{\top}\mathsf{T}\,dv, \tag{6.1}$$

and often referred to as the internal force vector. Here we have used matrix notation, where $\mathsf{R}_{\mathbf{u}}$ is the element displacement residual vector, B the standard "B-matrix" (often referred to as the symmetric discrete gradient matrix), and T the Cauchy "stress vector." In the following sections specific forms for $\mathsf{R}_{\mathbf{u}}, \mathsf{B}$, and T are provided for plane strain, axisymmetric, and three dimensional elements. Further, the corresponding displacement tangent (3.9) is often evaluated in the form

$$\mathsf{K}_{\mathbf{uu}} = \int_{\mathcal{B}^e} \mathsf{G}^{\top}\mathsf{A}\mathsf{G}\,dv, \tag{6.2}$$

with G the non-symmetric discrete gradient matrix, and A the matrix form of the spatial tangent modulus $\mathbb{A}$. Details also to follow for the specific element types considered.

Remark. The lengthy, but standard, computation for the displacement residual (3.9) is presented here for completeness. Restating the displacement residual

$$R^A_{u_i} = -\int_{\mathcal{B}^e}\left(\frac{\partial N^A}{\partial x_j}T_{ij}\right)dv.$$

Now, using the identities $dv = J\,dv_{\mathrm{R}}$, the definition of the Kirchhoff stress $\boldsymbol{\tau} = J\mathbf{T} = \mathbf{T}_{\mathrm{R}}\mathbf{F}^{\top}$, together with the identity $\mathbf{F}^{-\top}\nabla\varphi = \operatorname{grad}\varphi$ for a scalar field φ, we may recast the residual in the referential form

$$R^A_{u_i} = -\int_{\mathcal{B}^e}\frac{\partial N^A}{\partial X_a}F^{-1}_{aj}\tau_{ij}\,dv_{\mathrm{R}}. \tag{6.3}$$

Now, using $(3.8)_1$, and the identities

$$F_{mn} = \delta_{mn} + \sum u^B_m\frac{\partial N^B}{\partial X_n},\quad \frac{\partial F^{-1}_{ji}}{\partial F_{kl}} = -F^{-1}_{li}F^{-1}_{jk},\quad \text{and}\quad \frac{\partial N^A}{\partial x_i} = F^{-1}_{ai}\frac{\partial N^A}{\partial X_a},$$

we have

$$\begin{aligned}
K^{AB}_{u_iu_k} &= -\frac{\partial R^A_{u_i}}{\partial u^B_k} = \int_{\mathcal{B}^e}\frac{\partial N^A}{\partial X_a}\left(\frac{\partial F^{-1}_{aj}}{\partial F_{mn}}\tau_{ij} + F^{-1}_{aj}\frac{\partial \tau_{ij}}{\partial F_{mn}}\right)\frac{\partial F_{mn}}{\partial u^B_k}dv_{\mathrm{R}}\\
&= \int_{\mathcal{B}^e}\frac{\partial N^A}{\partial X_a}\left(\frac{\partial F^{-1}_{aj}}{\partial F_{mn}}\tau_{ij} + F^{-1}_{aj}\frac{\partial \tau_{ij}}{\partial F_{mn}}\right)\frac{\partial N^B}{\partial X_n}\delta_{mk}dv_{\mathrm{R}}\\
&= \int_{\mathcal{B}^e}\frac{\partial N^A}{\partial X_a}\left(-F^{-1}_{nj}F^{-1}_{am}\tau_{ij} + F^{-1}_{aj}\frac{\partial \tau_{ij}}{\partial F_{mn}}\right)\frac{\partial N^B}{\partial X_n}\delta_{mk}dv_{\mathrm{R}}\\
&= \int_{\mathcal{B}^e}\frac{\partial N^A}{\partial X_a}\left(-F^{-1}_{ak}F^{-1}_{nj}\tau_{ij} + F^{-1}_{aj}\frac{\partial \tau_{ij}}{\partial F_{kn}}\right)\frac{\partial N^B}{\partial X_n}dv_{\mathrm{R}}\\
&= \int_{\mathcal{B}^e}\frac{\partial N^A}{\partial x_j}F_{ja}\left(-F^{-1}_{ak}F^{-1}_{nj}\tau_{ij} + F^{-1}_{aj}\frac{\partial \tau_{ij}}{\partial F_{kn}}\right)F_{ln}\frac{\partial N^B}{\partial x_l}dv_{\mathrm{R}}\\
&= \int_{\mathcal{B}^e}\frac{\partial N^A}{\partial x_j}\left(-\delta_{jk}\tau_{il} + F_{ln}\frac{\partial \tau_{ij}}{\partial F_{kn}}\right)\frac{\partial N^B}{\partial x_l}dv_{\mathrm{R}}\\
&= \int_{\mathcal{B}^e}\frac{\partial N^A}{\partial x_j}\left(-J^{-1}\delta_{jk}\tau_{il} + J^{-1}F_{ln}\frac{\partial \tau_{ij}}{\partial F_{kn}}\right)\frac{\partial N^B}{\partial x_l}dv\\
&= \int_{\mathcal{B}^e}\frac{\partial N^A}{\partial x_j}\left(-J^{-1}\delta_{jk}\tau_{il} + J^{-1}F_{ln}F_{jm}\frac{\partial T_{\mathrm{R},im}}{\partial F_{kn}} + J^{-1}F_{ln}T_{\mathrm{R},im}\delta_{jk}\delta_{mn}\right)\frac{\partial N^B}{\partial x_l}dv\\
&= \int_{\mathcal{B}^e}\frac{\partial N^A}{\partial x_j}\left(-J^{-1}\delta_{jk}\tau_{il} + J^{-1}F_{ln}F_{jm}\frac{\partial T_{\mathrm{R},im}}{\partial F_{kn}} + J^{-1}\delta_{jk}\tau_{il}\right)\frac{\partial N^B}{\partial x_l}dv\\
&= \int_{\mathcal{B}^e}\frac{\partial N^A}{\partial x_j}\left(J^{-1}F_{ln}F_{jm}\frac{\partial T_{\mathrm{R},im}}{\partial F_{kn}}\right)\frac{\partial N^B}{\partial x_l}dv
\end{aligned}$$

or with

$$\mathbb{A}_{ijkl} \overset{\text{def}}{=} J^{-1}F_{jm}F_{ln}(\mathbb{A}_{\mathrm{R}})_{imkn},\quad \text{with}\quad \mathbb{A}_{\mathrm{R}} \overset{\text{def}}{=} \frac{\partial \mathbf{T}_{\mathrm{R}}}{\partial \mathbf{F}} \tag{6.4}$$

defining a *spatial tangent modulus*, we arrive at

$$K^{AB}_{u_iu_k} = \int_{\mathcal{B}^e}\frac{\partial N^A}{\partial x_j}(\mathbb{A}_{ijkl})\frac{\partial N^B}{\partial x_l}dv. \tag{6.5}$$

□

To accommodate both compressible and nearly incompressible material behavior and mitigate *volumetric locking* behavior, we have implemented the so called *F-bar* method (de Souza Neto et al., 1996). This method is based on replacing the deformation gradient suitably such that the incompressibility constraint is enforced as an approximate average throughout the element,

rather than point wise at each integration point. The method is based on the distortional-volumetric split of the deformation gradient

$$\mathbf{F} = \mathbf{F}_{\text{dis}}\mathbf{F}_{\text{vol}}, \tag{6.6}$$

with

$$\mathbf{F}_{\text{dis}} = J^{-1/3}\mathbf{F}, \quad \mathbf{F}_{\text{vol}} = J^{1/3}\mathbf{1}. \tag{6.7}$$

To construct the modified deformation gradient at an integration point of interest, we first determine the deformation gradient at the centroid of the element, denoted by $\mathbf{F}_c$. Then the modified deformation gradient is constructed as

$$\bar{\mathbf{F}} = \left(\frac{\det \mathbf{F}_c}{\det \mathbf{F}}\right)^{1/3}\mathbf{F}. \tag{6.8}$$

Now when computing the stresses at the integration points, the modified deformation gradient $\bar{\mathbf{F}}$ is substituted in place of $\mathbf{F}$. This has the effect that all the integration points in the element share the same total volumetric deformation gradient in the element, specifically $\det \mathbf{F}_c$. This formulation does not change the integration point residual computation (6.1), simply that $\bar{\mathbf{F}}$ is used to compute the constitutive response, rather than $\mathbf{F}$. However, the tangent computation (6.2) must be modified to

$$\mathsf{K}_{\mathbf{uu}} = \underbrace{\int_{\mathcal{B}^e} \mathsf{G}^{\top}\mathsf{A}\mathsf{G}\,dv}_{\text{standard terms}} + \underbrace{\int_{\mathcal{B}^e} \mathsf{G}^{\top}\mathsf{Q}(\mathsf{G}_0 - \mathsf{G})\,dv}_{\text{additional terms}}, \tag{6.9}$$

with

$$\mathbb{Q} = \frac{1}{3}\mathbb{A} : (\mathbf{1}\otimes\mathbf{1}) - \frac{2}{3}\mathbf{T}\otimes\mathbf{1}. \tag{6.10}$$

We have developed a 4-node quadrilateral two-dimensional plane-strain element, a 4-node quadrilateral axisymmetric element, and an 8-node brick three-dimensional element. The basic element technology of each is overviewed in the following subsections.

A.2. 2D elements

For the two-dimensional elements developed, the node ordering in the natural coordinates is shown in Fig. 8. Referring to Fig. 8, the shape functions for the 4-node linear element with respect to the natural coordinates are given by

$$N^1 = \frac{1}{4}(1-\xi)(1-\eta)$$
$$N^2 = \frac{1}{4}(1+\xi)(1-\eta)$$
$$N^3 = \frac{1}{4}(1+\xi)(1+\eta)$$
$$N^4 = \frac{1}{4}(1-\xi)(1+\eta).$$

A.2.1. Plane-strain

For a plane-strain element we have the condition that $F_{33} = 1$, and $F_{13} = F_{31} = F_{23} = F_{32} = 0$. Also, the B-matrix is given by

$$\mathsf{B} = \begin{bmatrix} \frac{\partial N^1}{\partial x_1} & 0 & \frac{\partial N^2}{\partial x_1} & 0 & \cdots & \frac{\partial N^M}{\partial x_1} & 0 \\ 0 & \frac{\partial N^1}{\partial x_2} & 0 & \frac{\partial N^2}{\partial x_2} & \cdots & 0 & \frac{\partial N^M}{\partial x_2} \\ \frac{\partial N^1}{\partial x_2} & \frac{\partial N^1}{\partial x_1} & \frac{\partial N^2}{\partial x_2} & \frac{\partial N^2}{\partial x_1} & \cdots & \frac{\partial N^M}{\partial x_2} & \frac{\partial N^M}{\partial x_1} \end{bmatrix} \tag{6.11}$$

where M is the total number of nodes in the element, and the stress vector T is given by

$$\mathsf{T} = [T_{11}\ T_{22}\ T_{12}]^{\top}. \tag{6.12}$$

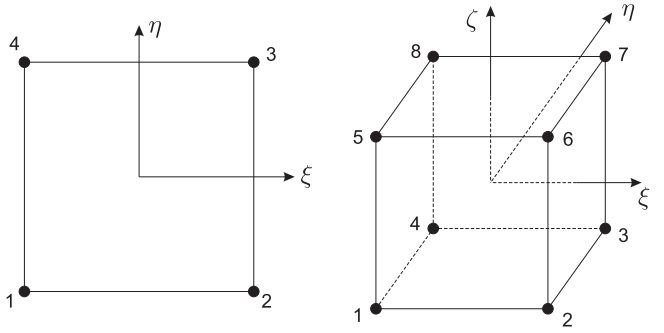

Fig. 8. Two-dimensional linear quadrilateral, and three-dimensional linear brick isoparametric master elements, with the node numbering as shown.

As mentioned before, to accommodate nearly incompressible material behavior where appropriate we use the F-bar method of de Souza Neto et al. (1996). Specifically in plane-strain the method reduces to

$$\begin{bmatrix} \bar{F}_{11} & \bar{F}_{12} & 0 \\ \bar{F}_{21} & \bar{F}_{22} & 0 \\ 0 & 0 & 1 \end{bmatrix} = \left(\frac{F_{c,11}F_{c,22} - F_{c,12}F_{c,21}}{F_{11}F_{22} - F_{12}F_{21}}\right)^{1/2} \begin{bmatrix} F_{11} & F_{12} & 0 \\ F_{21} & F_{22} & 0 \\ 0 & 0 & 1 \end{bmatrix}, \tag{6.13}$$

with $F_{c,ij}$ the deformation gradient at the centroid of the element. Correspondingly, in plane-strain, the tangent modification (6.9) is now given by

$$\mathbb{Q} = \frac{1}{2}\mathbb{A} : (\mathbf{1}\otimes\mathbf{1}) - \frac{1}{2}\mathbf{T}\otimes\mathbf{1} \tag{6.14}$$

where

$$[\mathbb{A} : (\mathbf{1}\otimes\mathbf{1})] = \begin{bmatrix} A_{11}+A_{14} & 0 & 0 & 0 & A_{11}+A_{14} \\ A_{21}+A_{24} & 0 & 0 & 0 & A_{21}+A_{24} \\ A_{31}+A_{34} & 0 & 0 & 0 & A_{31}+A_{34} \\ A_{41}+A_{44} & 0 & 0 & 0 & A_{41}+A_{44} \end{bmatrix} \tag{6.15}$$

with

$$\mathsf{A}_{mn} = \mathbb{A}_{ijkl}$$

denoting the matrix representation of $\mathbb{A}$ using the following transformation table

m/n	i/k	j/l
1	1	1
2	2	1
3	1	2
4	2	2

and with

$$[\mathbf{T}\otimes\mathbf{1}] = \begin{bmatrix} T_{11} & 0 & 0 & 0 & T_{11} \\ T_{21} & 0 & 0 & 0 & T_{21} \\ T_{12} & 0 & 0 & 0 & T_{12} \\ T_{22} & 0 & 0 & 0 & T_{22} \end{bmatrix} \tag{6.16}$$

for the plane-strain formulation. Finally, the standard non-symmetric discrete gradient matrix in (6.9) is given by

$$\mathsf{G} = \begin{bmatrix} \frac{\partial N^1}{\partial x_1} & 0 & \frac{\partial N^2}{\partial x_1} & 0 & \cdots & \frac{\partial N^M}{\partial x_1} & 0 \\ 0 & \frac{\partial N^1}{\partial x_1} & 0 & \frac{\partial N^2}{\partial x_1} & \cdots & 0 & \frac{\partial N^M}{\partial x_1} \\ \frac{\partial N^1}{\partial x_2} & 0 & \frac{\partial N^2}{\partial x_2} & 0 & \cdots & \frac{\partial N^M}{\partial x_2} & 0 \\ 0 & \frac{\partial N^1}{\partial x_2} & 0 & \frac{\partial N^2}{\partial x_2} & \cdots & 0 & \frac{\partial N^M}{\partial x_2} \end{bmatrix}$$

in plane strain with M the total number of nodes.

A.2.2. Axisymmetric

For an axisymmetric element we have the condition that $F_{13} = F_{31} = F_{23} = F_{32} = 0$, and $F_{33} = R/R_0$. Furthermore, the integration is now modified such that $\int_{B^e} dxdy \rightarrow \int_{B^e} 2\pi r dr dz$. In the numerical implementation F_{33} is computed as R/R_0, and numerically this is accomplished by

$$R = \sum N^A x_1^A, \tag{6.17}$$

$$R_0 = \sum N^A X_1^A, \tag{6.18}$$

where x_1^A are the current 1-coordinates of the nodes, and X_1^A are the reference 1-coordinates of the nodes. Note that this scheme automatically implies that our axisymmetric element formulation assumes the radial direction is the 1-direction. Also, the B-matrix is given by

$$\mathsf{B} = \begin{bmatrix} \frac{\partial N^1}{\partial x_1} & 0 & \frac{\partial N^2}{\partial x_1} & 0 & \cdots & \frac{\partial N^M}{\partial x_1} & 0 \\ 0 & \frac{\partial N^1}{\partial x_2} & 0 & \frac{\partial N^2}{\partial x_2} & \cdots & 0 & \frac{\partial N^M}{\partial x_2} \\ \frac{\partial N^1}{\partial x_2} & \frac{\partial N^1}{\partial x_1} & \frac{\partial N^2}{\partial x_2} & \frac{\partial N^2}{\partial x_1} & \cdots & \frac{\partial N^M}{\partial x_2} & \frac{\partial N^M}{\partial x_1} \\ \frac{N^1}{R} & 0 & \frac{N^2}{R} & 0 & \cdots & \frac{N^M}{R} & 0 \end{bmatrix} \tag{6.19}$$

where M is the total number of nodes in the element, and the stress vector T is given by

$$\mathsf{T} = [T_{11}\ T_{22}\ T_{12}\ T_{33}]^\top. \tag{6.20}$$

As mentioned before, to accommodate nearly incompressible material behavior the F-bar method of de Souza Neto et al. (1996) is implemented, where the modified deformation gradient is given by (6.8), viz.,

$$\bar{\mathbf{F}} = \left(\frac{\det \mathbf{F}_c}{\det \mathbf{F}}\right)^{1/3} \mathbf{F}, \tag{6.21}$$

where both F_{33} and F_{c33} are computed before applying the F-bar method. The tangents need to be corrected according to (6.9) with

$$[\mathbb{A} : (\mathbf{1} \otimes \mathbf{1})] = \begin{bmatrix} A_{11}+A_{14}+A_{15} & 0 & 0 & A_{11}+A_{14}+A_{15} & A_{11}+A_{14}+A_{15} \\ A_{21}+A_{24}+A_{25} & 0 & 0 & A_{21}+A_{24}+A_{25} & A_{21}+A_{24}+A_{25} \\ A_{31}+A_{34}+A_{35} & 0 & 0 & A_{31}+A_{34}+A_{35} & A_{31}+A_{34}+A_{35} \\ A_{41}+A_{44}+A_{45} & 0 & 0 & A_{41}+A_{44}+A_{45} & A_{41}+A_{44}+A_{45} \\ A_{51}+A_{54}+A_{55} & 0 & 0 & A_{51}+A_{54}+A_{55} & A_{51}+A_{54}+A_{55} \end{bmatrix} \tag{6.22}$$

where

$$\mathsf{A}_{mn} = \mathbb{A}_{ijkl}$$

using the following transformation table

m/n	i/k	j/l
1	1	1
2	2	1
3	1	2
4	2	2
5	3	3

and with

$$[\mathbf{T} \otimes \mathbf{1}] = \begin{bmatrix} T_{11} & 0 & 0 & T_{11} & T_{11} \\ T_{21} & 0 & 0 & T_{21} & T_{21} \\ T_{12} & 0 & 0 & T_{12} & T_{12} \\ T_{22} & 0 & 0 & T_{22} & T_{22} \\ T_{33} & 0 & 0 & T_{33} & T_{33} \end{bmatrix} \tag{6.23}$$

for the axisymmetric formulation. Finally, the standard non-symmetric discrete gradient matrix in (6.9) is given by

$$\mathsf{G} = \begin{bmatrix} \frac{\partial N^1}{\partial x_1} & 0 & \frac{\partial N^2}{\partial x_1} & 0 & \cdots & \frac{\partial N^M}{\partial x_1} & 0 \\ 0 & \frac{\partial N^1}{\partial x_1} & 0 & \frac{\partial N^2}{\partial x_1} & \cdots & 0 & \frac{\partial N^M}{\partial x_1} \\ \frac{\partial N^1}{\partial x_2} & 0 & \frac{\partial N^2}{\partial x_2} & 0 & \cdots & \frac{\partial N^M}{\partial x_2} & 0 \\ 0 & \frac{\partial N^1}{\partial x_2} & 0 & \frac{\partial N^2}{\partial x_2} & \cdots & 0 & \frac{\partial N^M}{\partial x_2} \\ \frac{N^1}{R} & 0 & \frac{N^2}{R} & 0 & \cdots & \frac{N^M}{R} & 0 \end{bmatrix}$$

with M the total number of nodes.

A.3. Three dimensional element

For the three-dimensional 8-node linear brick element developed the node ordering in the natural coordinates is shown in Fig. 8. Referring to Fig. 8, the shape functions for the 8-node linear brick element with respect to the natural coordinates are given by

$$N^1 = \frac{1}{8}(1-\xi)(1-\eta)(1-\zeta), \quad N^2 = \frac{1}{8}(1+\xi)(1-\eta)(1-\zeta),$$
$$N^3 = \frac{1}{8}(1+\xi)(1+\eta)(1-\zeta), \quad N^4 = \frac{1}{8}(1-\xi)(1+\eta)(1-\zeta),$$
$$N^5 = \frac{1}{8}(1-\xi)(1-\eta)(1+\zeta), \quad N^6 = \frac{1}{8}(1+\xi)(1-\eta)(1+\zeta),$$
$$N^7 = \frac{1}{8}(1+\xi)(1+\eta)(1+\zeta), \quad N^8 = \frac{1}{8}(1-\xi)(1+\eta)(1+\zeta).$$

Here the B-matrix is given by

$$\mathsf{B} = \begin{bmatrix} \frac{\partial N^1}{\partial x_1} & 0 & 0 & \frac{\partial N^2}{\partial x_1} & 0 & 0 & \cdots & \frac{\partial N^M}{\partial x_1} & 0 & 0 \\ 0 & \frac{\partial N^1}{\partial x_2} & 0 & 0 & \frac{\partial N^2}{\partial x_2} & 0 & \cdots & 0 & \frac{\partial N^M}{\partial x_2} & 0 \\ 0 & 0 & \frac{\partial N^1}{\partial x_3} & 0 & 0 & \frac{\partial N^2}{\partial x_3} & \cdots & 0 & 0 & \frac{\partial N^M}{\partial x_3} \\ \frac{\partial N^1}{\partial x_2} & \frac{\partial N^1}{\partial x_1} & 0 & \frac{\partial N^2}{\partial x_2} & \frac{\partial N^2}{\partial x_1} & 0 & \cdots & \frac{\partial N^M}{\partial x_2} & \frac{\partial N^M}{\partial x_1} & 0 \\ 0 & \frac{\partial N^1}{\partial x_3} & \frac{\partial N^1}{\partial x_2} & 0 & \frac{\partial N^2}{\partial x_3} & \frac{\partial N^2}{\partial x_2} & \cdots & 0 & \frac{\partial N^M}{\partial x_3} & \frac{\partial N^M}{\partial x_2} \\ \frac{\partial N^1}{\partial x_3} & 0 & \frac{\partial N^1}{\partial x_1} & \frac{\partial N^2}{\partial x_3} & 0 & \frac{\partial N^2}{\partial x_1} & \cdots & \frac{\partial N^M}{\partial x_3} & 0 & \frac{\partial N^M}{\partial x_1} \end{bmatrix} \tag{6.24}$$

where M is the total number of nodes in the element, and the stress vector T is given by

$$\mathsf{T} = [T_{11}\ T_{22}\ T_{33}\ T_{12}\ T_{23}\ T_{13}]^\top. \tag{6.25}$$

To accommodate nearly incompressible material behavior the F-bar method of de Souza Neto et al. (1996) as described above is implemented through

$$\bar{\mathbf{F}} = \left(\frac{\det \mathbf{F}_c}{\det \mathbf{F}}\right)^{1/3} \mathbf{F}, \tag{6.26}$$

The tangents need to be corrected according to (6.9) with

$$[\mathbb{A} : (\mathbf{1} \otimes \mathbf{1})] = \begin{bmatrix} A_{11}+A_{15}+A_{19} & 0 & 0 & 0 & A_{11}+A_{15}+A_{19} & 0 & 0 & 0 & A_{11}+A_{15}+A_{19} \\ A_{21}+A_{25}+A_{29} & 0 & 0 & 0 & A_{21}+A_{25}+A_{29} & 0 & 0 & 0 & A_{21}+A_{25}+A_{29} \\ A_{31}+A_{35}+A_{39} & 0 & 0 & 0 & A_{31}+A_{35}+A_{39} & 0 & 0 & 0 & A_{31}+A_{35}+A_{39} \\ A_{41}+A_{45}+A_{49} & 0 & 0 & 0 & A_{41}+A_{45}+A_{49} & 0 & 0 & 0 & A_{41}+A_{45}+A_{49} \\ A_{51}+A_{55}+A_{59} & 0 & 0 & 0 & A_{51}+A_{55}+A_{59} & 0 & 0 & 0 & A_{51}+A_{55}+A_{59} \\ A_{61}+A_{65}+A_{69} & 0 & 0 & 0 & A_{61}+A_{65}+A_{69} & 0 & 0 & 0 & A_{61}+A_{65}+A_{69} \\ A_{71}+A_{75}+A_{79} & 0 & 0 & 0 & A_{71}+A_{75}+A_{79} & 0 & 0 & 0 & A_{71}+A_{75}+A_{79} \\ A_{81}+A_{85}+A_{89} & 0 & 0 & 0 & A_{81}+A_{85}+A_{89} & 0 & 0 & 0 & A_{81}+A_{85}+A_{89} \\ A_{91}+A_{95}+A_{99} & 0 & 0 & 0 & A_{91}+A_{95}+A_{99} & 0 & 0 & 0 & A_{91}+A_{95}+A_{99} \end{bmatrix} \tag{6.27}$$

where

$$\mathsf{A}_{mn} = \mathbb{A}_{ijkl}$$

using the following transformation table

m/n	i/k	j/l
1	1	1
2	2	1
3	3	1
4	1	2
5	2	2
6	3	2
7	1	3
8	2	3
9	3	3

and with

$$[\mathbf{T}\otimes\mathbf{1}] = \begin{bmatrix} T_{11} & 0 & 0 & 0 & T_{11} & 0 & 0 & 0 & T_{11} \\ T_{21} & 0 & 0 & 0 & T_{21} & 0 & 0 & 0 & T_{21} \\ T_{31} & 0 & 0 & 0 & T_{31} & 0 & 0 & 0 & T_{31} \\ T_{12} & 0 & 0 & 0 & T_{12} & 0 & 0 & 0 & T_{12} \\ T_{22} & 0 & 0 & 0 & T_{22} & 0 & 0 & 0 & T_{22} \\ T_{32} & 0 & 0 & 0 & T_{32} & 0 & 0 & 0 & T_{32} \\ T_{13} & 0 & 0 & 0 & T_{13} & 0 & 0 & 0 & T_{13} \\ T_{23} & 0 & 0 & 0 & T_{23} & 0 & 0 & 0 & T_{23} \\ T_{33} & 0 & 0 & 0 & T_{33} & 0 & 0 & 0 & T_{33} \end{bmatrix} \tag{6.28}$$

for the three-dimensional formulation. Finally, the standard non-symmetric discrete gradient matrix in (6.9) is given by

$$\mathsf{G} = \begin{bmatrix} \frac{\partial N^1}{\partial x_1} & 0 & 0 & \frac{\partial N^2}{\partial x_1} & 0 & 0 & \cdots & \frac{\partial N^M}{\partial x_1} & 0 & 0 \\ 0 & \frac{\partial N^1}{\partial x_1} & 0 & 0 & \frac{\partial N^2}{\partial x_1} & 0 & \cdots & 0 & \frac{\partial N^M}{\partial x_1} & 0 \\ 0 & 0 & \frac{\partial N^1}{\partial x_1} & 0 & 0 & \frac{\partial N^2}{\partial x_1} & \cdots & 0 & 0 & \frac{\partial N^M}{\partial x_1} \\ \frac{\partial N^1}{\partial x_2} & 0 & 0 & \frac{\partial N^2}{\partial x_2} & 0 & 0 & \cdots & \frac{\partial N^M}{\partial x_2} & 0 & 0 \\ 0 & \frac{\partial N^1}{\partial x_2} & 0 & 0 & \frac{\partial N^2}{\partial x_2} & 0 & \cdots & 0 & \frac{\partial N^M}{\partial x_2} & 0 \\ 0 & 0 & \frac{\partial N^1}{\partial x_2} & 0 & 0 & \frac{\partial N^2}{\partial x_2} & \cdots & 0 & 0 & \frac{\partial N^M}{\partial x_2} \\ \frac{\partial N^1}{\partial x_3} & 0 & 0 & \frac{\partial N^2}{\partial x_3} & 0 & 0 & \cdots & \frac{\partial N^M}{\partial x_3} & 0 & 0 \\ 0 & \frac{\partial N^1}{\partial x_3} & 0 & 0 & \frac{\partial N^2}{\partial x_3} & 0 & \cdots & 0 & \frac{\partial N^M}{\partial x_3} & 0 \\ 0 & 0 & \frac{\partial N^1}{\partial x_3} & 0 & 0 & \frac{\partial N^2}{\partial x_3} & \cdots & 0 & 0 & \frac{\partial N^M}{\partial x_3} \end{bmatrix}$$

with M the total number of nodes.

Appendix B. Verification of the basic element technology

Since typical multi-physics problems are difficult to solve analytically, in this section we briefly compare a few numerical solutions with those that we can compute either analytically or by using an accepted solution method for a model system. Due to the complexity of the coupling, we consider it sufficient for this paper to verify the pure deformation problem and the pure diffusion problem, separately.

B.1. The deformation only problem

In the absence of a fluid, the constitutive theory reduces to that of a compressible neo-Hookean material with the Cauchy stress

$$\mathbf{T} = J^{-1}[G(\mathbf{B}-\mathbf{1}) + K\ln(J)\mathbf{1}].$$

To approximate a nearly incompressible neo-Hookean material we take $K = 10^3 G$. We use this constitutive equation to verify our UELs for the deformation only problem. For the corresponding analytical solutions considered below, we assume complete incompressibility ($J = 1$) and in this case the corresponding Cauchy stress for a neo-Hookean material is given by

$$\mathbf{T} = G\mathbf{B} - P\mathbf{1},$$

with P a constitutively indeterminate pressure, which is introduced to satisfy the incompressibility constraint.

For simple compression in the $\mathbf{e}_1$-direction, the analytical solution for the stress-stretch behavior is given by

$$T_{11} = G(\lambda^2 - \lambda^{-1}).$$

This analytical solution is compared against corresponding results computed by using a single U3D8 element, and a single UAX4 element in Fig. 9(a), in which the solid line represents the analytical solution and the symbols the numerically calculated results.

In plane strain compression in the $\mathbf{e}_1$-direction with no deformation in the $\mathbf{e}_3$-direction, the analytical solution for the stress-stretch behavior is given by

$$T_{11} = G(\lambda^2 - \lambda^{-2}).$$

This analytical solution also compared in Fig. 9(a) against the corresponding result computed by using a single UPE4 element; the dashed line represents the analytical solution, and the symbols the numerically calculated result.

Next, we examine the response in simple shear. Fig. 9(b) compares the analytical results for the shear stress and normal stress difference given by

$$T_{12} = G\gamma \quad \text{and} \quad T_{11} - T_{33} = G\gamma^2,$$

where γ is the amount of shear, against the numerical results computed using a single U3D8 element. Again, the solid and dashed lines represent the analytical solutions, and the symbols the numerically calculated result.

The results shown in Fig. 9 verify our basic element technology when dealing with large mechanical deformations in the absence of diffusion of the solvent.

B.2. The diffusion only problem

To verify the diffusion component of our finite elements, we use the classical analogy between the diffusion of a chemical species in a body and the diffusion of heat in a body, and consider the energy balance in a deformable heat conductor as our governing partial differential equation,

$$\dot{\vartheta} = \alpha\,\mathrm{div}(\mathrm{grad}\,\vartheta),$$

where α is the thermal diffusivity of the material. We compare results form a UEL implementation for this problem against the corresponding widely-accepted results obtained from the built-in thermo-mechanical elements in ABAQUS/Standard (2013). We consider the initial geometry as shown in Fig. 10, with the initial condition $\vartheta_0 = 300$ K everywhere in the body. We take the thermal diffusivity α to be a constant equal to 1×10^{-6} m^2/s.

In order to examine the UEL capabilities as thoroughly as possible, we consider the following two-step simulation;

- In the first step, the body is deformed isothermally using displacement boundary conditions.
- In the second step, the displacement boundary conditions are held fixed, and then the thermal boundary conditions are changed such that the transient heat equation discussed above is solved on the deformed body.

Referring to Fig. 10, in the first isothermal deformation step, the nodes along face AD are fixed, while nodes along face BC are prescribed a displacement to deform the body, while the temperature

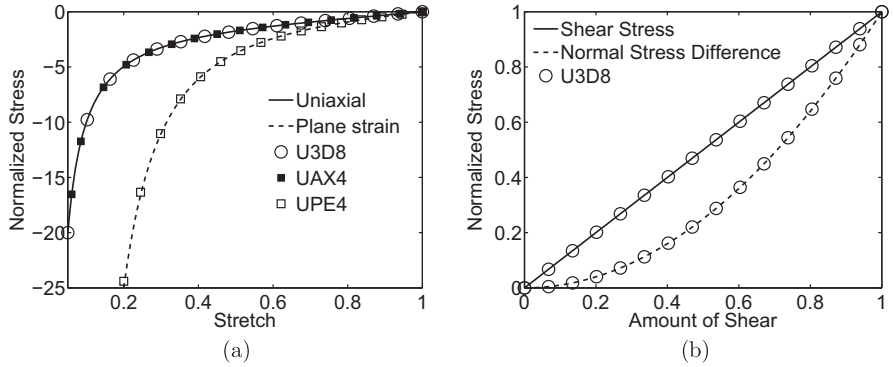

Fig. 9. Comparison of numerical solutions against analytical solutions for the deformation only problem: (a) Normalized stress T_{11}/G versus stretch λ behavior in simple compression as well as plane strain compression. (b) Normalized stress T_{12}/G and normalized stress-difference $(T_{11} - T_{33})/G$ versus amount of shear γ in simple shear. In all cases the lines represent the analytical solution and markers the finite element solution.

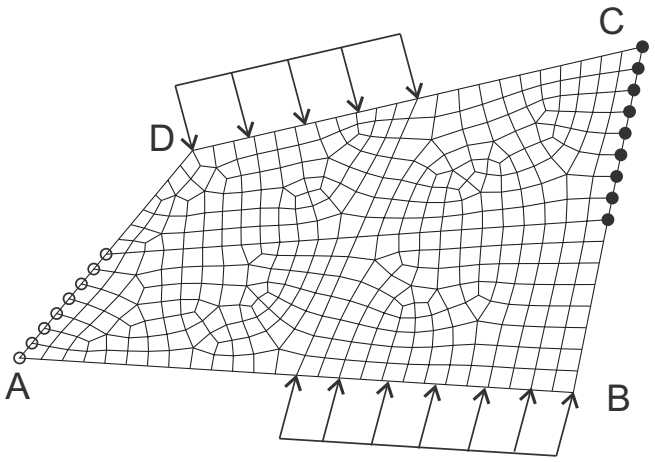

Fig. 10. Mesh and boundary conditions used in the verification of the diffusion component of the UEL. The temperature is prescribed on the nodes indicated on faces AD and BC, while fluxes are prescribed on the portions of faces as shown.

is still fixed at 300 K everywhere. In the second step, for the mechanical boundary conditions the nodes along faces AD and BC are held fixed. For the thermal boundary conditions, nodes on face AD held fixed at 300 K (the open circles in Fig. 10) and nodes on face BC (the filled circles in Fig. 10) are ramped from 300 K to 350 K over 100 s. Further, we prescribe a flux of (i) -0.01 W/m^2 on the indicated portion of face AB; and (ii) 0.02 W/m^2 on the indicated portion of face CD. All thermal flux boundary conditions are applied instantaneously at the start of the step.

The numerical simulation is performed using built-in ABAQUS elements, as well as our user elements for both plane strain and axisymmetric geometries. Fig. 11 shows the nodal temperature field on the deformed body after 500 s of simulation time with the outline of the initial body superimposed. Fig. 12 shows the temperature of the mid-side node on faces AB and CD.

These results verify our basic element technology when dealing with a transient diffusion only problem for plane strain and axisymmetric geometries. We have performed a similar analysis using our three dimensional elements, however for brevity, the results are not presented here.

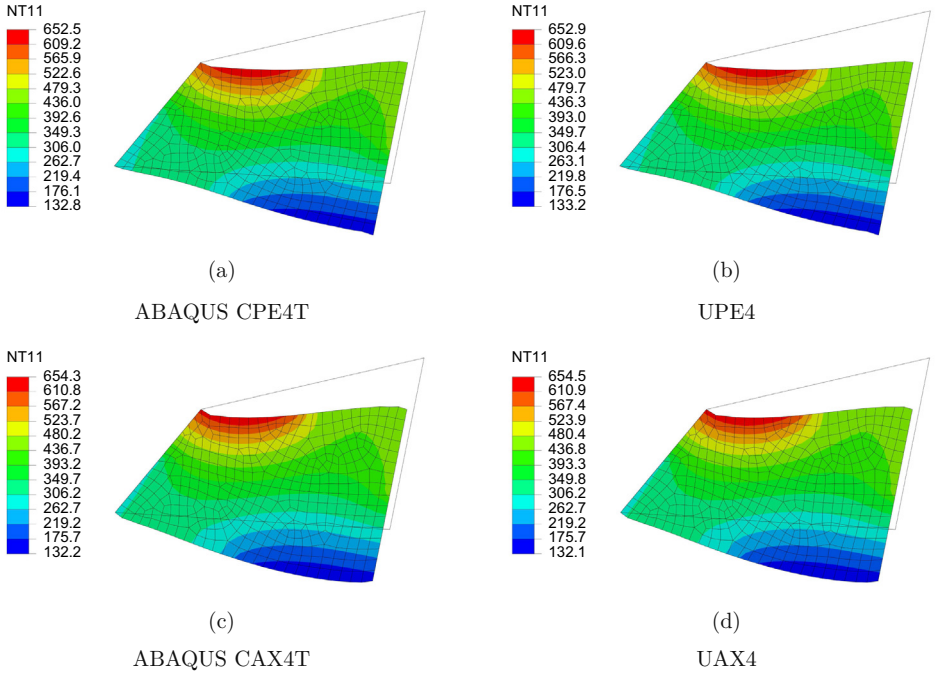

Fig. 11. Nodal temperature field in degrees K after 500 s of simulation time for (a) an ABAQUS CPE4T, (b) a UPE4, (c) an ABAQUS CAX4T, and lastly (d) a UAX4 element.

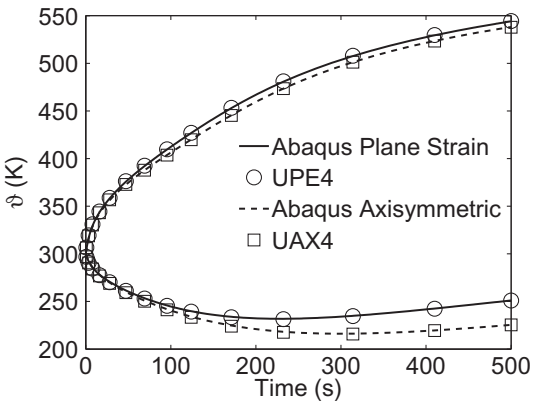

Fig. 12. Temperature as a function of time for the mid-side node on faces AB and CD. Lines indicate the simulations using the built in ABAQUS elements, while markers indicate the UEL.

Appendix C. A thermo-chemo-mechanically coupled theory

With the aim of aiding other researchers in their development of UEL capabilities, in this appendix we summarize an extension of the theory presented in Section 2 aimed at modeling thermally responsive gels. In this situation, one must consider not only the displacement and the chemical potential fields, but also the temperature field. Within the Abaqus framework, such a coupled set of PDE's is most readily solved using the UEL capability. In addition to the theory summarized here, we have included the source code and relevant associated files in the online Supplemental materials.

C.1. Summary of the theory

C.1.1. Constitutive equations

In what follows we neglect thermal expansion effects since they are small compared to the large volume changes due to the inflow/outflow of solvent in the body. The constitutive equations of the thermo-chemo-mechanically coupled theory are:

- *Free energy*: A simple form of the free energy function which accounts for the combined effects of mixing, swelling, and elastic stretching is,

$$\psi_{\mathrm{R}} = \mu^0 c_{\mathrm{R}} + R\vartheta c_{\mathrm{R}}\left(\ln\left(\frac{\Omega c_{\mathrm{R}}}{1+\Omega c_{\mathrm{R}}}\right)+\chi\left(\frac{1}{1+\Omega c_{\mathrm{R}}}\right)\right) + \frac{1}{2}G\left(3(\bar{\lambda}^2-1)-2\ln J\right)+J^s\left[\frac{1}{2}K(\ln J^e)^2\right]+f(\vartheta). \tag{8.1}$$

  Here, $G(\vartheta)=N_{\mathrm{R}}k_B\vartheta$ is the temperature dependent shear modulus of the network with N_{R} the number of polymer chains per reference volume, k_B the Boltzmann constant, and ϑ the absolute temperature. The term $f(\vartheta)$ is related to the specific heat of the material and we leave it unspecified here.

  Next, we specialize the temperature dependence of the chi-parameter $\chi(\vartheta)$ in the Flory–Huggins expression (8.1) for the free energy of mixing. Recall that this parameter represents the disaffinity between the polymer and the solvent—if $\chi(\vartheta)$ is increased, the fluid molecules are expelled from the gel and the gel shrinks, while if $\chi(\vartheta)$ is decreased, the gel absorbs more fluid and swells. Typically, thermally-responsive gels possess a critical transition temperature, ϑ_T, and exhibit a larger degree of swelling at temperatures below ϑ_T than at temperatures above ϑ_T (e.g., Gotoh et al., 1998; Afroze et al., 2000; Xue et al., 2001; Zhang et al., 2003; Liu et al., 2008). To model such experimentally-observed phenomena we assume that

$$\chi(\vartheta)=\frac{1}{2}(\chi_L+\chi_H)-\frac{1}{2}(\chi_L-\chi_H)\tanh\left(\frac{\vartheta-\vartheta_T}{\Delta}\right) \tag{8.2}$$

  where ϑ_T is the transition temperature of the gel, χ_L is the value of χ below the transition temperature, $\chi_H>\chi_L$ is the value of χ above the transition temperature, with Δ the width of the transition in temperatures between χ_L and χ_H.[7]

- *Constitutive equation for the Cauchy stress*: Corresponding to the free energy (8.1), the Cauchy stress $\mathbf{T}$ is given by

$$\mathbf{T}=J^{-1}\left(2\mathbf{F}^e\frac{\partial\psi_{\mathrm{R}}}{\partial\mathbf{C}^e}\mathbf{F}^{e\top}\right)=J^{-1}\left[G(\mathbf{B}-\mathbf{1})+J^sK(\ln J^e)\mathbf{1}\right]. \tag{8.3}$$

- *Constitutive equation for the chemical potential*: The chemical potential μ is given by

$$\mu=\frac{\partial\psi_{\mathrm{R}}}{\partial c_{\mathrm{R}}}-\Omega\frac{1}{3}J^e\mathrm{tr}\mathbf{T}=\mu^0+R\vartheta\left(\ln(1-\phi)+\phi+\chi\phi^2\right) -\Omega K(\ln J^e)+\frac{1}{2}K\Omega(\ln J^e)^2. \tag{8.4}$$

- *Constitutive equation for the fluid flux*: We assume that the spatial fluid flux, $\mathbf{j}$, depends linearly on the spatial gradient of the chemical potential, $\mathrm{grad}\,\mu$, with the mobility tensor taken to be isotropic so that

$$\mathbf{j}=-m\,\mathrm{grad}\,\mu, \tag{8.5}$$

  where m is a scalar mobility coefficient, we assume m in the same form as (4.1).

- *Constitutive equation for the heat flux*: We assume that the spatial heat flux, $\mathbf{q}$, depends linearly on the spatial gradient of the temperature, $\mathrm{grad}\,\vartheta$, with the thermal conductivity tensor taken to be isotropic so that

$$\mathbf{q}=-k\,\mathrm{grad}\,\vartheta, \tag{8.6}$$

  where k is the scalar thermal conductivity, which for simplicity is taken to be constant.

C.1.2. Governing partial differential equations

The governing partial differential equations, when expressed in the deformed body, consist of

1. The local force balance for the macroscopic Cauchy stress,

$$\mathrm{div}\mathbf{T}+\mathbf{b}=\mathbf{0}, \tag{8.7}$$

   with $\mathbf{b}$ a non-inertial body force, and $\mathbf{T}$ given by (2.9).
2. The local balance for the fluid concentration,

$$\frac{\dot{\phi}}{J\Omega\phi^2}-\mathrm{div}\mathbf{j}=0, \tag{8.8}$$

   in which the fluid flux $\mathbf{j}$ is given by (8.5), and the chemical potential μ is given by (8.4).
3. The local energy balance for the temperature,

$$c\dot{\vartheta}+\mathrm{div}\,\mathbf{q}=h \tag{8.9}$$

   where the heat flux is given by (8.6), c is the specific heat (per unit volume), and h is the contribution due to any source/sink terms. Readers are referred to Chester and Anand (2011) for more details on the specific contributions to h, in what follows here, we neglect any such contributions and set $h=0$.

C.1.3. Boundary and initial conditions

We also need boundary and initial conditions to complete the theory. Let $\mathcal{S}_{\mathbf{u}}$ and $\mathcal{S}_{\mathbf{t}}$ be complementary subsurfaces of the

[7] Other models have also been developed in an effort to capture the temperature and fluid concentration dependence on thermal responsiveness in the literature, (c.f., e.g., Cai and Suo, 2011).

boundary $\partial\mathcal{B}$ of the body $\mathcal{B}$ in the sense $\partial\mathcal{B} = \mathcal{S}_{\mathbf{u}} \cup \mathcal{S}_{\mathbf{t}}$ and $\mathcal{S}_{\mathbf{u}} \cap \mathcal{S}_{\mathbf{t}} = \varnothing$. Similarly let $\mathcal{S}_\mu$ and $\mathcal{S}_{\mathbf{j}}$ be complementary subsurfaces of the boundary: $\partial\mathcal{B} = \mathcal{S}_\mu \cup \mathcal{S}_{\mathbf{j}}$ and $\mathcal{S}_\mu \cap \mathcal{S}_{\mathbf{j}} = \varnothing$. And lastly let $\mathcal{S}_\vartheta$ and $\mathcal{S}_{\mathbf{q}}$ be complementary subsurfaces of the boundary: $\partial\mathcal{B} = \mathcal{S}_\vartheta \cup \mathcal{S}_{\mathbf{q}}$ and $\mathcal{S}_\vartheta \cap \mathcal{S}_{\mathbf{q}} = \varnothing$. Then for a time interval $t \in [0, T]$ we consider a pair of boundary conditions in which the displacement $\mathbf{u}$ is specified on $\mathcal{S}_{\mathbf{u}}$ and the surface traction on $\mathcal{S}_{\mathbf{t}}$:

$$\left.\begin{aligned} \mathbf{u} &= \breve{\mathbf{u}} \quad \text{on } \mathcal{S}_{\mathbf{u}} \times [0,T], \\ \mathbf{T}\mathbf{n} &= \breve{\mathbf{t}} \quad \text{on } \mathcal{S}_{\mathbf{t}} \times [0,T]; \end{aligned}\right\} \tag{8.10}$$

a pair of boundary conditions in which the chemical potential is specified on $\mathcal{S}_\mu$ and the fluid flux on $\mathcal{S}_{\mathbf{j}}$

$$\left.\begin{aligned} \mu &= \breve{\mu} \quad \text{on } \mathcal{S}_\mu \times [0,T], \\ -\mathbf{j}\cdot\mathbf{n} &= \breve{j} \quad \text{on } \mathcal{S}_{\mathbf{j}} \times [0,T]; \end{aligned}\right\} \tag{8.11}$$

and a pair of boundary conditions in which the temperature is specified on $\mathcal{S}_\vartheta$ and the heat flux on $\mathcal{S}_{\mathbf{q}}$

$$\left.\begin{aligned} \vartheta &= \breve{\vartheta} \quad \text{on } \mathcal{S}_\vartheta \times [0,T], \\ -\mathbf{q}\cdot\mathbf{n} &= \breve{q} \quad \text{on } \mathcal{S}_{\mathbf{q}} \times [0,T]; \end{aligned}\right\} \tag{8.12}$$

with $\breve{\mathbf{u}}, \breve{\mathbf{t}}, \breve{\mu}, \breve{j}, \breve{\vartheta}$, and $\breve{q}$, *prescribed* functions of $\mathbf{x}$ and t. The initial data is taken as

$$\begin{aligned} &\mathbf{u}(\mathbf{X},0) = \mathbf{u}_0(\mathbf{X}), \quad \text{and} \quad \mu(\mathbf{X},0) = \mu_0(\mathbf{X}) \quad \text{and} \\ &\vartheta(\mathbf{X},0) = \vartheta_0(\mathbf{X}) \quad \text{in B}. \end{aligned} \tag{8.13}$$

The coupled set of Eqs. (8.7), (8.8), and (8.9), together with (8.10), (8.11), (8.12), and (8.13) yield an initial boundary value problem for the displacement $\mathbf{u}(\mathbf{x}, t)$, the chemical potential $\mu(\mathbf{x}, t)$, and the temperature $\vartheta(\mathbf{x}, t)$.

C.2. Numerical solution procedure

In this section, since the basic procedure follows from Section 3, we only highlight and summarize the major points of modification. The full details may be found in the source code and input files, which are provided with the online Supplemental materials.

In the absence of body forces, the strong forms of the coupled partial differential equations consist of the balance of forces, as well as the balance of fluid content as described in (3.1), however now we also append the balance of energy, which is the heat equation,

$$\text{Balance of energy} \begin{cases} c\dot{\vartheta} + \operatorname{div}\mathbf{q} = 0 & \text{in } \mathcal{B}, \\ \vartheta = \breve{\vartheta} & \text{on } \mathcal{S}_\vartheta, \\ -\mathbf{q}\cdot\mathbf{n} = \breve{q} & \text{on } \mathcal{S}_{\mathbf{q}}. \end{cases} \tag{8.14}$$

Then, with $\mathbf{w}_1, w_2$, and w_3 denoting three weighting (or test) fields which vanish on $\mathcal{S}_{\mathbf{u}}, \mathcal{S}_\mu$, and $\mathcal{S}_\vartheta$ respectively, the corresponding weak forms are:

$$\left.\begin{aligned} &\int_{\mathcal{B}} \left(\mathbf{T} : \frac{\partial \mathbf{w}_1}{\partial \mathbf{x}}\right) dv = \int_{\mathcal{S}_{\mathbf{t}}} (\mathbf{w}_1 \cdot \breve{\mathbf{t}}) da, \\ &\int_{\mathcal{B}} \left(w_2 \frac{\dot{\phi}}{J\Omega\phi^2}\right) dv = -\int_{\mathcal{B}} \left(\frac{\partial w_2}{\partial \mathbf{x}} \cdot \mathbf{j}\right) dv - \int_{\mathcal{S}_{\mathbf{j}}} \left(w_2 \breve{j}\right) da, \\ &\int_{\mathcal{B}} (w_3 c\dot{\vartheta}) dv = \int_{\mathcal{B}} \left(\frac{\partial w_3}{\partial \mathbf{x}} \cdot \mathbf{q}\right) dv + \int_{\mathcal{S}_{\mathbf{q}}} (w_3 \breve{q}) da. \end{aligned}\right\} \tag{8.15}$$

The body is approximated using finite elements, $\mathcal{B} = \bigcup \mathcal{B}^e$, and the trial solutions for the displacement, chemical potential, and temperature are interpolated inside each element by

$$\left.\begin{aligned} \mathbf{u} &= \sum \mathbf{u}^A N^A, \\ \mu &= \sum \mu^A N^A, \\ \vartheta &= \sum \vartheta^A N^A, \end{aligned}\right\} \tag{8.16}$$

with the index $A = \{1, 2, \ldots, M\}$ denoting the nodes of the element, $\mathbf{u}^A$, μ^A, and ϑ^A denoting nodal displacements, chemical potentials, and temperatures, and N^A the shape functions. We employ a standard Galerkin approach, in that the weighting fields are interpolated by the same shape functions, viz.

$$\left.\begin{aligned} \mathbf{w}_1 &= \sum \mathbf{w}_1^A N^A, \\ w_2 &= \sum w_2^A N^A, \\ w_3 &= \sum w_3^A N^A. \end{aligned}\right\} \tag{8.17}$$

This leads to the system of coupled equations is solved using a Newton procedure by defining the following element-level residuals for the displacement, chemical potential, and temperature,

$$\left.\begin{aligned} (R_{u_i})^A &= -\int_{\mathcal{B}^e} \left(T_{ij} \frac{\partial N^A}{\partial x_j}\right) dv + \int_{\mathcal{S}_{\mathbf{t}}^e} \left(N^A \breve{t}_i\right) da, \\ (R_\mu)^A &= \int_{\mathcal{B}^e} \left(N^A \frac{\dot{\phi}}{J\Omega\phi^2}\right) dv - \int_{\mathcal{B}^e} \left(m \frac{\partial N^A}{\partial x_i} \frac{\partial \mu}{\partial x_i}\right) dv + \int_{\mathcal{S}_{\mathbf{j}}^e} \left(N^A \breve{j}\right) da, \\ (R_\vartheta)^A &= \int_{\mathcal{B}^e} \left(N^A c\dot{\vartheta}\right) dv + \int_{\mathcal{B}^e} \left(k \frac{\partial N^A}{\partial x_i} \frac{\partial \vartheta}{\partial x_i}\right) dv - \int_{\mathcal{S}_{\mathbf{j}}^e} \left(N^A \breve{q}\right) da. \end{aligned}\right\} \tag{8.18}$$

In addition to the residuals, the following tangents are also required for the iterative Newton solver:

$$\left.\begin{aligned} (\mathbf{K}_{\mathbf{uu}})^{AB} &= -\tfrac{\partial (\mathbf{R}_{\mathbf{u}})^A}{\partial \mathbf{u}^B}, \quad (\mathbf{K}_{\mu\mathbf{u}})^{AB} = -\tfrac{\partial (R_\mu)^A}{\partial \mathbf{u}^B}, \quad (\mathbf{K}_{\vartheta\mathbf{u}})^{AB} = -\tfrac{\partial (R_\vartheta)^A}{\partial \mathbf{u}^B}, \\ (\mathbf{K}_{\mathbf{u}\mu})^{AB} &= -\tfrac{\partial (\mathbf{R}_{\mathbf{u}})^A}{\partial \mu^B}, \quad (K_{\mu\mu})^{AB} = -\tfrac{\partial (R_\mu)^A}{\partial \mu^B}, \quad (K_{\vartheta\mu})^{AB} = -\tfrac{\partial (R_\vartheta)^A}{\partial \mu^B}, \\ (\mathbf{K}_{\mathbf{u}\vartheta})^{AB} &= -\tfrac{\partial (\mathbf{R}_{\mathbf{u}})^A}{\partial \vartheta^B}, \quad (K_{\mu\vartheta})^{AB} = -\tfrac{\partial (R_\mu)^A}{\partial \vartheta^B}, \quad (K_{\vartheta\vartheta})^{AB} = -\tfrac{\partial (R_\vartheta)^A}{\partial \vartheta^B}. \end{aligned}\right\} \tag{8.19}$$

Details of each of the tangents listed above may be found in the source code.

C.3. Numerical example

To demonstrate the robustness of the developed user element subroutine in simulating thermo-chemo-mechanically coupled problems in this section we provide an illustrative numerical simulation. This example problem uses the same geometry and mesh as shown in Fig. 4 for the constrained bilayer swelling (bending) used previously in Section 4.2.

For this example a two-step simulation is implemented; the first step is identical to the isothermal swelling as described in Section 4.2 and shown in Fig. 5, while in the second step the temperature is varied and heat is conducted into the gel causing deswelling. For the first step of the simulation we keep the same

Table 2
Material parameters for a representative thermally responsive elastomeric gel.

Parameter	Value
N_R	2.43×10^{25} /m^3
$G = N_R k_B \vartheta$ (at 298 K)	1 MPa
K	100 MPa
Ω	1.0×10^{-4} m^3/mol
χ_L	0.1
χ_H	0.7
ϑ_T	320 K
Δ	5.0 K
μ^0	0.0 J/mol
D	5×10^{-9} m^2/s
c	4.18×10^6 J/(m^3 K)
k	0.5 W/(m K)

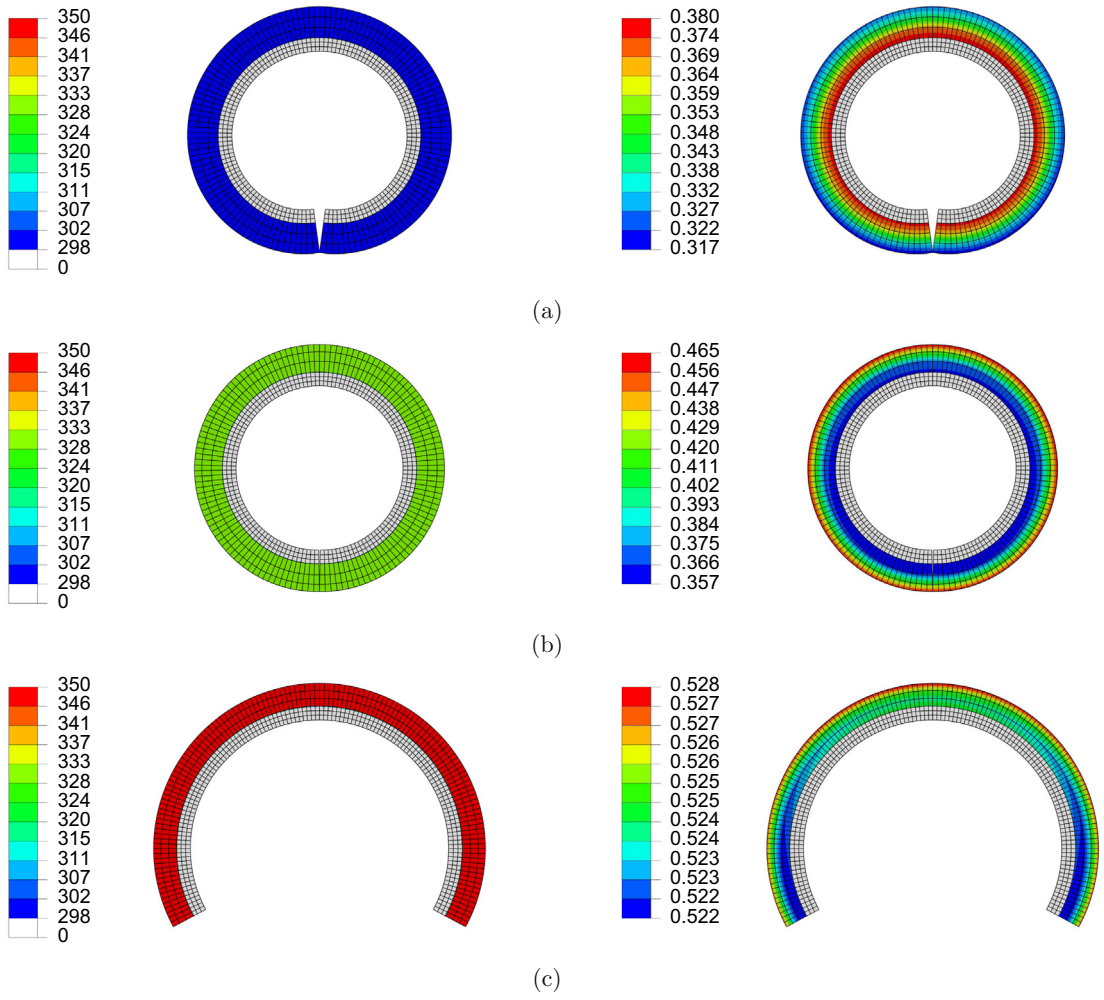

Fig. 13. Contours of the temperature ϑ (left, in degrees Kelvin) and polymer volume fraction ϕ (right) at (a) the start, (b) 4 h, and (c) 12 h in the second step of the simulation. Here the unfurling of the bilayer is due to the thermal responsiveness of the gel as the temperature is raised to 350 K.

mechanical and chemical boundary conditions as in Section 4.2 however we now impose the initial condition on the temperature $\vartheta_0 = 298$ K over the entire body. Also, in the first step, nodes along face CD are prescribed $\breve{\vartheta} = 298$ K while the other faces, including the interface between the non-swellable substrate and gel, are prescribed zero heat flux. In the second step however, after six hours of swelling in the first step, nodes along face CD are prescribed a temperature increase to $\breve{\vartheta} = 350$ >K over 6 hours and the simulation is allowed to run for another 6 h. The other faces, including the interface are prescribed zero heat flux. *We note that the non-swellable substrate does not conduct heat nor diffuse solvent in this simulation.*

Table 2, which is based on Table 1, lists plausible representative values for the material properties of a *thermally responsive* polymeric gel, which we have used in the following calculation. Fig. 13 shows contours of the temperature and polymer volume fraction in the deforming body. From Fig. 13 the coupling between the temperature and degree of swelling is clearly visible. It is clear that the change in the temperature locally changes the chemistry, i.e., $\chi(\vartheta)$, which drives solvent out of the gel causing an unfurling of the bilayer. We note that since the layer is thin, and fluid diffuses much more slowly than heat, the temperature contours are nearly constant at any given instant of time.

This numerical example shows the use of our user elements in a thermo-chemo-mechanically coupled situation for simulating thermally responsive gels. Along with the online Supplemental materials this extra example should prove useful to researchers trying to adapt UEL's for their own use in other coupled problems.

Appendix D. Supplementary data

Supplementary data associated with this article can be found, in the online version, at http://dx.doi.org/10.1016/j.ijsolstr.2014.08.015.

References

ABAQUS/Standard, 2013. SIMULIA, Providence, RI.
Afroze, F., Nies, E., Berghmans, H., 2000. Phase transitions in the system poly(N-isopropylacrylamide)/water and swelling behaviour of the corresponding networks. J. Mol. Struct. 554, 55–68.
Al-Athela, K., Loeffel, K., Liu, H., Anand, L., 2013. Modeling decohesion of a top-coat from a thermally-growing oxide in a thermal barrier coating. Surf. Coat. Technol. 222, 68–78.
Anand, L., Aslan, O., Chester, S.A., 2012. A large-deformation gradient theory for elastic–plastic materials: strain softening and regularization of shear bands. Int. J. Plast. 30, 116–143.
Beebe, D.J., Moore, J.S., Auer, J.M., Yu, Q., Liu, R.H., Devadoss, C., Jo, B., 2000. Functional hydrogel structures for autonomous flow control inside microfluidic devices. Nature 404, 588–590.
Bhavsar, R., Vaidya, N.Y., Ganguly, P., Humphreys, A., Robisson, A., Tu, H., Wicks, N., McKinley, G.H., Pauchet, F., 2008. Intelligence in novel materials. Oilfield Rev. 20, 32–41.

Cai, S., Hu, Y., Zhao, X., Suo, Z., 2010. Poroelasticity of a covalently crosslinked alginate hydrogel under compression. J. Appl. Phys. 108, 113514.
Cai, S.Q., Suo, Z., 2011. Mechanics and chemical thermodynamics of phase transition in temperature-sensitive hydrogels. J. Mech. Phys. Solids 59, 2259–2278.
Chan, G., Mooney, D.J., 2008. Trends Biotechnol. 26, 382–392.
Chester, S.A., Anand, L., 2010. A coupled theory of fluid permeation and large deformations for elastomeric materials. J. Mech. Phys. Solids 58, 1879–1906.
Chester, S.A., Anand, L., 2011. A thermo-mechanically coupled theory for fluid permeation in elastomeric materials: application to thermally responsive gels. J. Mech. Phys. Solids 59, 1978–2006.
Chester, S.A., 2012. A constitutive model for coupled fluid permeation and large viscoelastic deformation in polymeric gels. Soft Matter 8, 8223–8233.
Di Leo, C.V., Anand, L., 2013. Hydrogen in metals: a coupled theory for species diffusion and large elastic-plastic deformations. Int. J. Plast. 43, 42–69.
Di Leo, C.V., Rejovitsky, E., Anand, L., 2014. A Cahn–Hilliard-type phase-field theory for species diffusion coupled with large elastic deformations: application to phase-separating Li-ion electrode materials. J. Mech. Phys. Solids 70, 1–29.
Doi, M., 2009. Gel dynamics. J. Phys. Soc. Jpn. 78, 052001.
Duan, Z., Zhang, J., An, Y., Jiang, H., 2013. Simulation of the transient behavior of gels based on an analogy between diffusion and heat transfer. J. Appl. Mech. 80, 041017.
Duda, F.P., Souza, A.C., Fried, E., 2010. A theory for species migration in finitely strained solid with application to polymer network swelling. J. Mech. Phys. Solids 58, 515–529.
de Souza Neto, E.A., Perić, D., Dutko, M., Owen, D.R.J., 1996. Design of simple low order finite elements for large strain analysis of nearly incompressible solids. Int. J. Solids Struct. 33, 3277–3296.
Giner, E., Sukumar, N., Tarancon, J.E., Fuenmayor, F.J., 2009. An ABAQUS implementation of the extended finite element method. Eng. Fract. Mech. 76, 347–368.
Gotoh, T., Nakatani, Y., Sakohara, S., 1998. Novel synthesis of thermosensitive porous hydrogels. J. Appl. Polym. Sci. 69, 895–906.
Gurtin, M.E., Fried, E., Anand, L., 2010. The Mechanics and Thermodynamics of Continua. Cambridge University Press, Cambridge.
Henann, D.L., Chester, S.A., Bertoldi, K., 2013. Modeling of dielectric elastomers: design of actuators and energy harvesting devices. J. Mech. Phys. Solids 61, 2047–2066.
Henann, D.L., Bertoldi, K., 2014. Modeling of elasto-capillary phenomena. Soft Matter 10, 709–717.
Holmes, D.P., Roche, M., Sinha, T., Stone, H.A., 2011. Bending and twisting of soft materials by non-homogenous swelling. Soft Matter 7, 5188.
Hong, W., Zhao, X., Zhou, J., Suo, Z., 2008. A theory of coupled diffusion and large deformation in polymeric gel. J. Mech. Phys. Solids 56, 1779–1793.
Hong, W., Liu, Z., Suo, Z., 2009. Inhomogeneous swelling of a gel in equilibrium with a solvent and mechanical load. Int. J. Solids Struct. 46, 3282–3289.
Kleverlaan, M., Van Hoort, R.H., Jones, I., 2005. Deployment of swelling elastomer packers in Shell E&P. In: SPIE/IADC Drilling Conference. Amsterdam.
Lee, H., Zhang, J., Jiang, H., Fang, N.X., 2012. Prescribed pattern transformation in swelling gel tubes by elastic instability. Phys. Rev. Lett. 108, 214304.
Liu, K., Ovaert, T.C., Mason, J.J., 2008. Preparation and mechanical characterization of a PNIPA hydrogel composite. J. Mater. Sci. Mater. Med. 19, 1815–1821.
Liu, Z., Hong, W., Suo, Z., Swaddiwudhipong, S., Zhang, Y., 2010. Modeling and simulation of buckling of polymeric membrane thin film gel. Comput. Mater. Sci. 49, 560–564.
Loeffel, K., Anand, L., Gasem, Z., 2013. On modeling the oxidation of high-temperature alloys. Acta Mater. 61, 399–424.
Lucantonio, A., Nardinocchi, P., Teresi, L., 2013. Transient analysis of swelling-induced large deformations in polymer gels. J. Mech. Phys. Solids 61, 205–218.
Marcombe, R., Cai, S., Hong, W., Zhao, X., Lapusta, Y., Suo, Z., 2010. A theory of constrained swelling of a pH-sensitive hydrogel. Soft Matter 6, 784–793.
Pandey, A., Holmes, D.P., 2013. Swelling-induced deformations: a materials-defined transition from macroscale to microscale deformations. Soft Matter 9, 5524.
Park, K., Paulino, G.H., 2012. Computational implementation of the PPR potential-based cohesive model in ABAQUS: educational perspective. Eng. Fract. Mech. 93, 239–262.
Peppas, N.A., Hilt, J.Z., Khademhosseini, A., Langer, R., 2006. Hydrogels in biology and medicine: from molecular principles to bionanotechnology. Adv. Mater. 18, 1345–1360.
Tanaka, T., Fillmore, D.J., 1979. Kinetics of swelling of gels. J. Chem. Phys. 70, 1214–1218.
Toh, W., Liu, S., Ng, T.Y., Hong, W., 2013. Inhomogeneous large deformation kinetics of polymeric gels. Int. J. Appl. Mech. 5, 1350001.
Xue, W., Champ, S., Huglin, M.B., 2001. New superabsorbent thermoreversable hydrogels. Polymer 42, 2247–2250.
Yoon, J., Cai, S., Suo, Z., Hayward, R.C., 2010. Poroelastic swelling kinetics of thin hydrogel layers: comparison of theory and experiment. Soft Matter 6, 6004–6012.
Zhang, X., Wang, F., Chu, C., 2003. Thermoresponsive hydrogel with rapid response dynamics. J. Mater. Sci. Mater. Med. 14, 451–455.
Zhang, J., Zhao, X., Suo, Z., Jiang, H., 2009. A finite element method for transient analysis of concurrent large deformation and mass transport in gels. J. Appl. Phys. 105, 093522.